



1  
2  
3  
4  
5  
6  
7  
8  
9  
10  
11  
12  
13  
14  
15  
16  
17  
18  
19  
20  
21  
22  
23  
24  
25  
26  
27  
28  
29  
30  
31  
32  
33  
34  
35

### **Introduction**

Traditionally, clinical medicine is organized by organ-centered disciplines which is reflected in the currently applied diagnostics and treatments of patients. This approach has been also commonly adopted in research strategies but it is becoming evident that novel interdisciplinary efforts are needed to improve therapies of complex diseases. For example Heart failure (HF) is a complex, debilitating condition afflicting millions of people worldwide (Savarese & Lund, 2017). However, in addition to the detrimental phenotypes linked directly to cardiac dysfunction, cognitive deficits present a major burden to patients with HF (Ampadu & Morley, 2015, Hajduk, Lemon et al., 2013, Pressler, Subramanian et al., 2010) (Doehner, Ural et al., 2017). Moreover, epidemiological studies have clearly demonstrated that HF significantly increases the risk for dementia and age-associated neurodegenerative diseases such as Alzheimer’s disease (AD) (Angermann, Frey et al., 2012, Cermakova, Lund et al., 2015, Satizabal, Beiser et al., 2016). In line with these observations, a consistent finding in HF patients is a substantially reduced cerebral blood flow (Roy, Woo et al., 2017) and imaging studies reveal subsequent structural and functional cerebral alterations including changes in key regions linked to memory formation, such as the hippocampus (Kumar, Woo et al., 2011) (Pan, Kumar et al., 2013) (Kumar, Yadav et al., 2015) (Woo, Ogren et al., 2015). However, how HF affects hippocampal function at the molecular level remains to be explored and thus effective therapies to manage cognitive impairment in HF patients do not exist yet. On the contrary, the therapeutic approaches currently used to treat cardiac phenotypes in HF patients lack evidence for improving cognition (Cleland, Daubert et al., 2005) (Arnold, Liu et al., 2006, Frigerio & Roubina, 2005) or have even been linked to an increased incidence of AD (Pressler et al., 2010) (Khachaturian, Zandi et al., 2006) (Galli & Lombardi, 2014) (Solomon, Rizkala et al., 2017), suggesting that HF may lead to long-lasting adaptive changes in neurons that can persist despite improvement of cardiac function. Thus, a better understanding of HF-mediated molecular alterations in neurons is of utmost importance but corresponding data is lacking. Consequently, international organizations such as the European Society of Cardiology (ESC) have recommended that cardiology and dementia research experts should team-up to identify therapeutic interventional options for managing cognitive impairment in subjects with HF (Ponikowski, Voors et al., 2018). In this study, we took on this challenge and show that heart failure leads to specific changes in hippocampal gene expression that are linked to memory impairment. Targeting aberrant gene expression via epigenetic drugs ameliorates these phenotypes suggesting a key role of this process in HF-mediated cognitive dysfunction. Moreover, our data suggest that therapeutic strategies directed towards epigenetic gene-expression provide a therapeutic avenue to improve cognition in HF patients and ameliorate their risk to develop AD.

1  
2  
3  
4  
5  
6  
7  
8  
9  
10  
11  
12  
13  
14  
15  
16  
17  
18  
19  
20  
21  
22  
23  
24  
25  
26  
27  
28  
29  
30  
31  
32  
33  
34

## Results

### *Heart failure in CamkII $\delta$ TG mice leads to hippocampal gene expression changes indicative of dementia*

With the aim to elucidate the molecular processes by which cardiovascular dysfunction leads to memory impairment and an increases the risk for dementia, we decided to employ a well-established mouse model for heart failure in which cardiomyocyte-specific kinase CamkII $\delta$  is overexpressed under the control of the alpha-MHC promoter (CamkII $\delta$  TG mice) (Maier, Zhang et al., 2003). Thus, overexpression of CamkII $\delta$  is specific to cardiomyocytes and is not detected in other organs, including the brain (Maier et al., 2003), making it a *bona fide* model to study the impact of heart failure on brain function (**Fig 1A**). We reasoned that this well-defined genetic heart failure model would be superior to other experimental approaches linked for example to cerebral hypoperfusion such as carotid artery occlusion, since it allowed us to study brain function in response to the very precise and exclusive manipulation of cardiac tissue. In line with previous findings, 3-month-old CamkII $\delta$  TG mice displayed heart failure with left ventricular dilatation, impaired ejection fraction, and increased heart mass (**Fig 1B, C**), whereas the overall body weight was not affected ( $P = 0.863$  for CamkII $\delta$  TG vs control mice,  $n = 8$ , unpaired  $t$ -test). As a first approach to study the impact of cardiac dysfunction on brain plasticity we decided to analyze the transcriptome of the hippocampal CA1 region in 3-month-old CamkII $\delta$  TG mice (**Fig 1D**). This was based on data showing that (1) gene expression is a sensitive molecular correlate of memory function and is de-regulated in dementia patients and corresponding mouse models (Fischer, 2014a); (2) the hippocampal CA1 regions is essential for spatial reference memory in rodents and humans and is affected early in AD (Fischer, 2014a) and (3) imaging data show functional changes of the hippocampal CA1 region in patients with HF (Woo et al., 2015). RNA-seq analysis revealed substantial changes in the CA1 transcriptome of 3-month old CamkII $\delta$  TG and control mice that were obvious in a principle component analysis (PCA; **Fig 1D**). Namely, 1780 genes were up-regulated and 2014 genes were down-regulated in CamkII $\delta$  TG when compared to the control group (**Fig. 1E**; supplemental table 1). Comparison of the differentially expressed genes to previously reported cell-type specific gene expression datasets (Merienne, Meunier et al., 2019) revealed that up-regulated genes were linked to neurons, microglia and astrocytes, while down-regulated genes were mainly associated with neurons (**Fig 1F**). Further pathway analysis showed that up-regulated genes are related to cellular stress response pathways such as oxidative and endoplasmic reticulum (ER) stress (**Fig. 1G**, supplemental table 1), while down-regulated genes are linked to cognition, protein folding and processes related to protein methylation (**Fig 1G**, supplemental table 1). We decided to confirm the RNA-sequencing data by testing differential

1 expression for selected genes representing changes related to increased cellular stress processes, in this  
2 case “ER stress“ and down-regulated processes such as “protein methylation”. qPCR analysis confirmed  
3 increased expression of the ER stress-related genes Fez1, Fez2 and Bcap31 (**Fig 1H**). We also tested the  
4 expression of several histone 3 lysine 4 (H3K4) specific lysine methyltransferases (Kmts), since these  
5 pathways were detected in the RNA-seq data and several of the Kmt’s, such as Kmt2a, were found to be  
6 essential for memory formation (Gupta, Kim et al., 2010, Kerimoglu, Agis-Balboa et al., 2013)  
7 (Jakovcevski, Ruan et al., 2015) (Kerimoglu, Sakib et al., 2017). Indeed, we observed that Kmt2a and  
8 Kmt2d were significantly down-regulated in CamkII $\delta$ c TG mice (**Fig 1H**). Specificity of this observation  
9 was demonstrated by the fact that other H3K4 methyltransferases such as Kmt2b and Kmt2c were not  
10 differentially expressed.

11 The observation that genes implicated with oxidative and ER stress are increased in the hippocampus of  
12 CamkII $\delta$ c TG mice is in line with previous findings linking heart failure to hypoxia as a consequence of  
13 cerebral hypoperfusion (Bikkina, Levy et al., 1994) (Verdecchia, Porcellati et al., 2001) (Perlman, 2007).  
14 The concomitant down-regulation of genes linked to cognition let us to hypothesize about a potential link  
15 between the observed cellular stress-related gene-expression changes and the decreased expression of  
16 genes associated with cognition. Namely, we wondered if the decreased expression of genes linked to  
17 cognition could be a consequence of the activation of cellular stress pathways. We decided to test this  
18 hypothesis further with a focus on hypoxia and ER-stress as key cellular stress pathways. Since data on  
19 the effects of hypoxia and ER-stress on hippocampal gene-expression at the genome-wide level is still  
20 rare, we decided to performed RNA-sequencing from mixed hippocampal neuronal cultures that were  
21 subjected to either hypoxia or ER-stress. First, we analyzed hypoxia. Differential expression analysis  
22 revealed a substantial amount of genes that were differentially expressed in response to hypoxic  
23 conditions (supplemental table 2). We then compared the genes up- and down-regulated in hippocampal  
24 cultures in response to hypoxia to the genes up- and down-regulated in the hippocampus of CamkII $\delta$ c TG  
25 mice. This analysis revealed a significant overlap of not only up - but also down-regulated genes  
26 suggesting that hypoxic conditions are sufficient to induce gene-expression changes similar to that  
27 detected in the hippocampus of mice suffering from HF (**Fig 1I**). We employed the same experimental  
28 settings to test the impact of ER-stress that can be modeled via the administration of tunicamycin. Thus,  
29 RNA-sequencing was performed from mixed hippocampal neuronal cultures upon treatment with  
30 tunicamycin (Supplemental table 3). Our data show that genes de-regulated in response to tunicamycin  
31 also significantly overlap with genes affected in CamkII $\delta$ c TG mice, although to a lesser extend when  
32 compared to hypoxia (**Fig 1I**). In sum, these data suggest a scenario in which heart failure that is linked to  
33 cerebral hypoperfusion leads to hypoxia, oxidative and ER-stress related hippocampal gene-expression  
34 changes which are upstream of the reduced expression of neuronal genes important for cognition. Taken

1 into account that impaired expression of genes essential for cognitive function is also a key hallmark of  
2 dementia, these data provide a plausible hypothesis to explain - at least in part – cognitive dysfunction in  
3 response to HF. To provide further evidence for this hypothesis, we first retrieved published datasets in  
4 which brain-specific gene-expression changes were reported in mouse models with impaired memory  
5 function, namely models for aging-associated memory decline (Benito, Urbanke et al., 2015), models for  
6 AD (Gjoneska, Pfenning et al., 2015) and Fronto-temporal dementia (FTLD) (Swarup, Hinz et al., 2018).  
7 We compared these datasets to the transcriptional alterations observed in the hippocampus of CamkII $\delta$ c  
8 TG mice (**Fig 1J**). Interestingly, there was a significant overlap of genes up-regulated in the hippocampus  
9 of CamkII $\delta$ c TG mice and genes up-regulated in the hippocampus of cognitively impaired old mice, in  
10 CK-p25 mice representing a model for AD-like neurodegeneration and in the cortex of FVB mice,  
11 representing a mouse model for fronto-temporal dementia FTLD (**Fig 1J**). Similarly, genes down-  
12 regulated in the hippocampus of CamkII $\delta$ c TG mice significantly overlapped with the genes down-  
13 regulated in models for aging, AD-like neurodegeneration and FTLD (**Fig 1J**).  
14 Thus, the hippocampal gene-expression signature observed in response to heart failure partly overlaps to  
15 the gene-expression changes detected in cognitive diseases. On this basis we hypothesized that aberrant  
16 hippocampal gene-expression and especially the decreased expression of learning and memory genes  
17 could be a central process in heart failure mediated cognitive impairment and might therefore represent a  
18 suitable target for therapeutic intervention. To further substantiate and test this hypothesis, we first  
19 decided to first analyze memory function in CamkII $\delta$ c TG mice directly.

20

21 ***Heart failure in CamkII $\delta$ c TG is associated with impaired hippocampus-dependent memory***  
22 ***consolidation.***

23 Three-month-old CamkII $\delta$ c TG (n=16) and control mice (n=13) were subjected to behavioral testing.  
24 Importantly, when subjected to the open field test, CamkII $\delta$ c TG and control mice traveled similar  
25 distances with the same speed, indicating that explorative behavior and basal motor-function is normal in  
26 CamkII $\delta$ c TG mice (**Fig 2A**). Both groups also spent similar time in the center of the open field arena,  
27 suggesting that anxiety behavior is not affected in CamkII $\delta$ c TG mice (**Fig 2A**). Subsequently, mice were  
28 subjected to the Barnes Maze, a hippocampus-dependent spatial navigation-learning test (see methods for  
29 details). Two-way ANOVA analysis revealed that CamkII $\delta$ c TG mice spent significantly more time to  
30 find the escape hole when compared to littermate controls (**Fig 2B**). These data suggest that  
31 hippocampus-dependent memory function is impaired in CamkII $\delta$ c TG mice. A detailed analysis of the  
32 different strategies to find the escape hole confirmed this observation and revealed that in comparison to  
33 control mice, CamkII $\delta$ c TG mice failed to adapt hippocampus-dependent strategies (direct, short and long  
34 chaining approaches), which are generally considered to depend on higher cognitive abilities than the

1 other strategies (**Fig. 2C**). To quantify this observation, we calculated the cumulative strategy score (see  
2 methods for details) that was significantly reduced in CamkII $\delta$ c TG mice when compared to the control  
3 group (**Fig 2D**), further confirming that CamkII $\delta$ c TG mice exhibit impaired hippocampus-dependent  
4 learning abilities. We also assayed memory retrieval 24h after the final day of training by placing the  
5 mice into the Barnes Maze arena with the escape hole being closed and measured the visits to the escape  
6 hole. The number of visits to the escape hole during the 120 sec test period was significantly lower in  
7 CamkII $\delta$ c TG mice when compared to the control group, indicating impaired retrieval of spatial memories  
8 (**Fig 2E**). In summary, these findings are in line with our gene-expression data (See Fig. 1) and show that  
9 CamkII $\delta$ c overexpression-induced heart failure leads to cognitive deficits.

10

### 11 *Heart failure-related down-regulation of hippocampal genes is linked to reduced neuronal H3K4-* 12 *methylation*

13 The finding that CamkII $\delta$ c mice indeed exhibit memory impairments allowed us to move on and explore  
14 our hypothesis that decreased expression of hippocampal learning and memory genes might be one of the  
15 underlying mechanisms by which heart failure leads to cognitive decline. Our gene-expression data  
16 suggest that genes down-regulated in the hippocampal CA1 region of CamkII $\delta$ c TG mice mainly reflect  
17 neuron-specific changes (See Figure 1F). In addition to pathways related to “cognition”, a major  
18 molecular process linked to these genes was protein methylation including down-regulation of H3K4-  
19 methyltransferases such as Kmt2a (see Fig 1H). Since reduced neuronal expression of Kmt2a and  
20 corresponding genome-wide reduction of H3K4me3 has been linked to memory impairment and AD  
21 (Gjoneska et al., 2015) (Kerimoglu et al., 2017), these data point to the possibility that altered H3K4-  
22 methylation may – at least in part – underlie the observed down-regulation of neuronal genes in CamkII $\delta$ c  
23 TG mice. To test this hypothesis, we retrieved and re-analyzed hippocampal RNA-seq data from mutant  
24 mice that lack the H3K4-methyltransferases Kmt2a or Kmt2b from hippocampal neurons of the adult  
25 brain and also display hippocampus-dependent memory impairment (Kerimoglu et al., 2013) (Kerimoglu  
26 et al., 2017). Our data reveal that genes decreased in CamkII $\delta$ c TG mice show a significant overlap with  
27 the genes affected in Kmt2a mutant mice (**Fig 3A**). In contrast, no significant overlap was seen when  
28 genes affected in CamkII $\delta$ c TG and Kmt2b mice were compared (**Fig 3A**). These findings are in line with  
29 the observation that Kmt2a but not Kmt2b is reduced in CamkII $\delta$ c TG mice and further supports the idea  
30 that changes in H3K4 methylation may contribute to decreased neuronal gene expression in CamkII $\delta$ c TG  
31 mice. To test this possibility directly, we decided to measure neuronal H3K4me3 in the hippocampal CA1  
32 region of CamkII $\delta$ c TG and control mice via chromatin-immunoprecipitation followed by next-generation  
33 sequencing (ChIP-seq). Tissue of the hippocampal CA1 region was processed and subjected to FACS to  
34 isolate neuronal nuclei using an established protocol (**Fig 3B**)(Benito et al., 2015, Halder, Hennion et al.,

1 2016). Afterwards H3K4me3 ChIP-seq was performed. We detected a total of 138026 H3K4me3 peaks  
2 across the entire genome. In line with previous findings from neuronal nuclei (Kerimoglu et al., 2017) and  
3 other tissues, the transcription start site (TSS) of genes was the major regulatory region where these peaks  
4 were localized (**Fig 3C**). When we compared H3K4me3 at the TSS of CamkII $\delta$ c TG and control mice we  
5 observed 4627 genes with decreased and 609 genes with significantly increased H3K4me3 peaks at the  
6 TSS (**Fig 3D**). It is important to reiterate that the ChIP-seq data stems specifically from neuronal nuclei of  
7 the hippocampal CA1 region allowing us to test the hypothesis that reduced neuronal H3K4me3 would  
8 explain the decreased expression of neuronal genes. Indeed, genes down-regulated in CamkII $\delta$ c TG (See  
9 Fig 1F, G) showed significantly reduced H3K4me3 level at their TSS (**Fig 3E**). In sum, these data  
10 provide strong evidence for the view that reduced neuronal H3K4me3 plays a crucial role in impaired  
11 neuronal gene expression observed in CamkII $\delta$ c TG mice and thereby contributes to heart failure induced  
12 memory loss.

13

#### 14 *Reinstating hippocampal gene-expression rescues memory impairment in CamkII $\delta$ c TG mice*

15 Our findings point to the possibility that therapeutic strategies to increase H3K4me3 may help to  
16 ameliorate cognitive impairment in CamkII $\delta$ c TG mice and could provide a novel approach to manage  
17 cognitive impairments in heart failure patients. H3K4me3 is a chromatin mark linked to active gene-  
18 expression and euchromatin conformation. Histone-deacetylase (HDAC) inhibitors increase histone-  
19 acetylation and thereby favor euchromatin formation. Moreover, administration of HDAC inhibitors  
20 could reinstate memory function in various mouse models of neurodegenerative diseases (Fischer, 2014b)  
21 and the HDAC inhibitor Vorinostat is currently tested as therapeutic intervention in AD patients  
22 (<https://clinicaltrials.gov/ct2/show/NCT03056495>). Notably, HDAC inhibitors were also found to  
23 reinstate hippocampal H3K4me3 and improve spatial reference learning in mice that lack the histone-  
24 methyltransferase Kmt2d (Bjornsson, Benjamin et al., 2014). On this basis we hypothesized that  
25 administration of Vorinostat might help to reinstate memory function in CamkII $\delta$ c TG mice, which would  
26 also provide further causal evidence for the role of altered neuronal gene-expression in HF-induced  
27 memory impairment. In a pilot experiment we found that Vorinostat was able to significantly enhance  
28 H3K9 acetylation and H3K4me3 - two euchromatin marks that are functionally related (Kerimoglu et al.,  
29 2013) (Kerimoglu et al., 2017, Stilling, Rönicke et al., 2014) - when administered to primary hippocampal  
30 neurons (**Expanded View 1**). Thus, 2-month-old CamkII $\delta$ c TG mice were treated with Vorinostat for 1  
31 month before behavioral testing. Another group of CamkII $\delta$ c TG mice received corresponding vehicle  
32 solution. Vehicle-treated wild type littermates served as additional control group (**Fig 4A**). All groups  
33 performed similarly in the open field test confirming our previous observation that CamkII $\delta$ c TG mice  
34 exhibit normal basal anxiety levels and motor function (**Fig 4B**). Moreover, Vorinostat had no effect on

1 these parameters. Next, mice were subjected to the Barnes Maze paradigm to evaluate spatial reference  
2 memory. Consistent with our previous observation, vehicle treated mice displayed impaired learning  
3 behavior when compared to the corresponding wild-type group (**Fig 4C**). In contrast, CamkII $\delta$ c TG mice  
4 treated with Vorinostat were able to master the Barnes Maze task similar to the wild type control group  
5 (**Fig 4C**). Essentially, the escape latency in Vorinostat-treated CamkII $\delta$ c TG and wild-type control groups  
6 was not significantly different, suggesting that Vorinostat administration reinstates hippocampus-  
7 dependent memory function in CamkII $\delta$ c TG mice (**Fig 4C**). A more detailed analysis of the training  
8 procedure revealed that similar to wild type mice, Vorinostat-treated CamkII $\delta$ c TG mice eventually adopt  
9 cognitive strategies such as direct, short and long chaining strategies, while vehicle-treated CamkII $\delta$ c TG  
10 failed to do so (**Fig 4D**). Consistently, the cumulative cognitive score that was calculated based on these  
11 strategies (*see* methods for details) revealed a significant impairment of vehicle-treated CamkII $\delta$ c TG  
12 mice, when compared to the wild-type control group, while no such difference was observed for  
13 Vorinostat-treated CamkII $\delta$ c TG (**Fig 4E**). A similar observation was made when mice were subjected to  
14 the memory test after 7 training trials (**Fig 4F**). These data show that oral administration of Vorinostat  
15 ameliorates memory impairment in CamkII $\delta$ c TG mice.

16

#### 17 *Vorinostat ameliorates gene-expression changes in CamkII $\delta$ c TG mice*

18 Vorinostat treatment of CamkII $\delta$ c TG mice had no significant effect on cardiac pathology (**Expanded**  
19 **View Fig 2**) suggesting that reinstatement of memory function in our experimental system is most likely  
20 linked to brain-specific processes. Thus, we analyzed gene-expression in the hippocampal CA1 region of  
21 vehicle-treated wild type mice as well as in vehicle and Vorinostat-treated CamkII $\delta$ c TG mice via RNA-  
22 seq (**Fig 5A**). In line with our previous observation (See Fig 1D-G), RNA-seq data analysis revealed a  
23 major deregulation of gene-expression in vehicle-treated CamkII $\delta$ c TG mice compared to the vehicle-  
24 treated wild-type control group (**Expanded View Fig 3A, B**). Our further analysis shows that Vorinostat  
25 could partially restore physiological gene-expression in CamkII $\delta$ c TG mice (**Expanded View Fig 3B, C**).  
26 The finding that Vorinostat-treatment increases the expression of genes that were down-regulated in  
27 CamkII $\delta$ c TG mice can easily be explained by the effect of Vorinostat on euchromatin formation.  
28 However, the observation that Vorinostat also decreases the expression of genes that were elevated in  
29 CamkII $\delta$ c TG mice is most likely due to additional mechanisms.

30 To further elucidate this, we decided to investigate the RNAseq data in greater detail. Recent studies  
31 showed that the detection of regulatory co-expression modules is a suitable approach to further  
32 understand transcriptional plasticity in health and disease (Gandal, Zhang et al., 2018). To this end we  
33 performed Weighted Gene Co-expression Analysis (Langfelder & Horvath, 2008) (**Fig 5B**) and identified  
34 14 different modules in the entire RNA-seq dataset (*see* methods for details). Two of these modules –



1 namely RNA module 1 and 2 - exhibited significantly different expression amongst vehicle-treated  
2 CamkII $\delta$  TG and wild-type control mice. RNA module 1 was decreased in vehicle-treated CamkII $\delta$  TG  
3 mice, while its expression was partially rescued upon Vorinostat treatment (**Fig 5C**). Gene ontology  
4 analysis suggested that the genes of RNA module 1 are linked to cognition, learning and memory (**Fig**  
5 **5C**). Further analysis identified a cluster of 30 hub genes within module 1. Notably, 26 of genes were  
6 shown to cause to memory impairment when their expression was manipulated (**Fig 5D**; supplemental  
7 table 4). In contrast, RNA module 2 was significantly increased in vehicle-treated CamkII $\delta$  TG mice  
8 when compared to the vehicle-treated wild-type control group (**Fig 5E**). Expression of this cluster was  
9 partially decreased to control levels in Vorinostat-treated CamkII $\delta$  TG mice (**Fig 5E**). In line with our  
10 previous analysis of up-regulated genes, the genes of RNA module 2 were mainly linked to cellular  
11 stress-related pathways (**Fig 5E**). In line with our previous findings the genes of RNA module 2 showed a  
12 significant overlap to genes increased in response to hypoxia in neuronal cultures (this study), human  
13 brain organoids exposed to hypoxia (Paşca, Park et al.) or ER-stress while the genes of the cognition-  
14 related RNA module 2 were decreased under the same conditions (**Expanded View Fig 4**).

15 The question remained how Vorinostat, an epigenetic drug that is linked to euchromatin formation and the  
16 activation of gene expression, would decrease the observed pathological gene-expression response linked  
17 to hypoxia and cellular stress pathways. One possible explanation is that Vorinostat induces molecular  
18 processes that antagonize this type of pathological gene expression. MicroRNAs are small non-coding  
19 RNAs that regulate cellular homeostasis via binding to a target mRNA thereby causing its degradation or  
20 inhibition of translation (Gurtan & Sharp, 2013). Compensatory microRNA responses have been  
21 described in response to various cellular stress conditions (Kagias, Nehammer et al., 2012) and we  
22 hypothesized that Vorinostat-induced microRNA expression might contribute to the therapeutic effect in  
23 CamkII $\delta$  TG mice. To this end, we performed small RNA sequencing of the hippocampal CA1 region  
24 obtained from control and vehicle-treated CamkII $\delta$  TG mice as well as from Vorinostat-treated  
25 CamkII $\delta$  TG mice. Differential expression analysis revealed a number of regulated microRNAs when  
26 comparing the various conditions (supplemental table 4). To specifically identify microRNA networks  
27 that could explain the decreased expression of cellular stress-response genes upon Vorinostat treatment,  
28 we performed a weighted co-expression analysis (Langfelder & Horvath, 2008) (**Fig 5G**) and identified 5  
29 microRNA modules (**Expanded View Fig 5 AB**). One module – namely microRNA module 2 - was  
30 significantly decreased in vehicle-treated CamkII $\delta$  TG mice when compared to the vehicle-control group  
31 (**Fig 5G**), while its expression was increased to physiological levels upon Vorinostat-treatment (**Fig 5G**).

32 Next, we asked whether the increased expression of microRNA module 2 would be correlated to the  
33 corresponding expression of stress-response genes increased in the hippocampal CA1 region of CamkII $\delta$   
34 TG mice. To this end we first performed a pairwise correlation analysis between genes and microRNAs

1 that were differentially expressed in Vorinostat-treated vs. vehicle-treated CamkII $\delta$ c TG mice. We  
2 observed that microRNAs within microRNA module 2 showed a significant negative correlation to the  
3 hub genes of RNA module 2, representing the module linked to cellular stress responses and autophagy  
4 (**Fig 5H**). These data suggest that Vorinostat-treatment in CamkII $\delta$ c TG mice increases the expression of  
5 microRNAs that antagonize the expression of genes linked to pathological cellular stress. Further  
6 evidence for this view stems from the finding that these microRNAs are mainly encoded within genes that  
7 exhibit reduced hippocampal H3K4me3 in CamkII $\delta$ c TG mice (**Expanded View Fig 5, C**).  
8 In sum these data suggest that aberrant neuronal gene expression plays a central role in heart failure  
9 associated cognitive decline. In turn, approaches that target these gene-expression changes could provide  
10 a novel therapeutic avenue to manage cognitive dysfunction in heart failure patients.

11

## 12 **Discussion**

13 Employing a genetic mouse model for HF, we show for the first time that HF leads to substantial changes  
14 in hippocampal gene expression. The genes that were up-regulated significantly overlap with genes  
15 deregulated in neurons exposed to cellular stress such as oxidative and ER stress. These data suggest that  
16 cardiac dysfunction, which has been linked to reduced blood flow to the brain (Bikkina et al., 1994,  
17 Verdecchia et al., 2001), initiates a cellular stress response that eventually manifest at the level of neural  
18 gene-expression. Our results also reveal that these hippocampal gene-expression changes in mice  
19 suffering from HF parallel the changes observed in models for neurodegenerative diseases (Benito et al.,  
20 2015) (Gjoneska et al., 2015) (Gispert, Brehm et al., 2015) (Swarup et al., 2018). This is in line with previous  
21 reports suggesting that hypoxia-mediated oxidative and ER-stress are early and common events in  
22 neurodegenerative diseases that can trigger subsequent pathological changes associated with memory loss  
23 (Feldstein, 2012) (Xiang, Wang et al., 2017) (Butterfield & Halliwell, 2019). Indeed, further analysis of  
24 the data revealed that the hippocampal genes down-regulated in response to heart failure represent cellular  
25 processes linked to cognition and are similar to the gene-expression changes observed in models for  
26 dementia. These findings suggest that activation of cellular stress pathways might be one reason for the  
27 down-regulation of hippocampal genes essential for cognition. Support for this view stems from our  
28 observation that the sole exposure of neuronal cultures to hypoxia or ER-stress leads to the down-  
29 regulation of such neuronal gene-sets. In line with these gene-expression data we show that CamkII $\delta$ c TG  
30 mice exhibit impaired hippocampus-dependent learning and memory. Although our report of memory  
31 impairment in a heart failure mouse model is novel, these data are in agreement with various studies in  
32 humans showing that cardiac dysfunction is associated with cognitive decline and an increased dementia  
33 risk (Angermann et al., 2012) (Ampadu & Morley, 2015) (Doehner et al., 2017). Furthermore, memory  
34 impairment has been reported in animal models for acute myocardial ischemia (Evonuk, Prabhu et al.,

1 2017) and various models for chronic cerebral hypoperfusion but the underlying molecular mechanisms  
2 remained poorly understood so far (e.g. see (Patel, Moalem et al., 2017)). How precisely activation of the  
3 various cellular stress pathways leads to the down-regulation of genes essential for cognition remains to  
4 be investigated and is likely to be multifactorial making it difficult to identify suitable targets for  
5 therapeutic intervention. From a therapeutic point of view, the fact that hippocampal genes linked to  
6 cognition are eventually decreased, might offer a more promising avenue to treat cognitive defects in HF  
7 patients, especially since these patients usually already suffer from the disease for a prolonged time  
8 period. In this context, it is important to reiterate that our data suggest that HF eventually leads to the  
9 down-regulation of gene-clusters important for cognition via processes linked to reduced histone-  
10 methylation, especially decreased levels of the euchromatin mark H3K4me3. These findings are in line  
11 with current literature showing that proper neuronal H3K4me3 is essential for memory consolidation  
12 (Gupta et al., 2010, Kerimoglu et al., 2013) (Jakovcevski et al., 2015) (Kerimoglu et al., 2017). Our data hint  
13 at a specific role of the H3K4 methyltransferase Kmt2a, which is down-regulated in the hippocampus of  
14 CamkII $\delta$  TG mice. These findings are in line with recent reports showing that mice lacking Kmt2A in  
15 excitatory neurons of the hippocampus exhibit impaired learning and memory and decreased expression  
16 of genes implicated in cognitive function (Kerimoglu et al., 2017). Indeed, our data show that genes  
17 deregulated in the hippocampi of Kmt2a knock out mice - but not of Kmt2b - significantly overlap with  
18 deregulated genes in CamkII $\delta$  TG mice. Taken together, these data point to a scenario in which heart  
19 failure leads to hypoxia and cellular stress, eventually driving loss of neuronal euchromatin causing  
20 decreased expression of neuronal plasticity genes essential for cognition (**Fig 6**). Further support for this  
21 view stems from our data that administration of an epigenetic drugs that promotes euchromatin formation  
22 reinstates memory in CamkII $\delta$  TG mice and that this effect cannot be simply explained by improved  
23 cardiac output. These findings pave the road to a novel therapeutic approach to treat HF-induced  
24 cognitive dysfunction and lower the risk for age-associated dementia in these patients. To this end,  
25 although cerebral hypoperfusion and cellular stress appear to be initial events in the development of  
26 cognitive decline in patients suffering for cardiac dysfunction, our data suggest that they eventually lead  
27 to epigenetic changes of histone methylation in neurons. Such epigenetic alterations are known to  
28 represent long-term adaptive changes that can persist even in the absence of the initial stimulus (Fischer,  
29 2014a). Thus, targeting the epigenome has emerged as a promising therapeutic option to treat complex  
30 and multifactorial diseases including dementia, even at an advanced stage of the disease (Fischer, 2014b)  
31 (Fischer, 2014a). In fact, previous studies showed that other risk factors for dementia such as aging  
32 (Peleg, Sananbenesi et al., 2010) (Benito et al., 2015), protein aggregation, (Kilgore, Miller et al., 2010)  
33 (Govindarajan, Agis-Balboa et al., 2011) (Benito et al., 2015) (Gjoneska et al., 2015), neuropsychiatric  
34 diseases (Nestler, Peña et al., 2015) or peripheral inflammation(Wendeln AC, Häsler LM et al., 2018)

1 lead to similar changes representing a loss of neuronal euchromatin and reduced expression of genes  
2 linked to cognition. Of note, therapeutic strategies to reinstate euchromatin related gene-expression were  
3 able to improve memory function in such models (Benito et al., 2015) (Bahari-Javan, Varbanov et al.,  
4 2017). For example, inhibitors of histone deacetylases (HDAC) have emerged as promising candidates to  
5 treat cognitive decline, and the FDA approved HDAC inhibitor Vorinostat is currently undergoing trials  
6 in Alzheimer's disease patients (ClinicalTrials.gov Identifier: NCT03056495). As mentioned above, oral  
7 administration of Vorinostat to CamkII $\delta$  TG mice improved their learning and memory abilities. These  
8 findings cannot be explained by improved cardiac function, since a one-month treatment of CamkII $\delta$  TG  
9 mice with Vorinostat had no significant effect on heart failure. However, Vorinostat treatment increased  
10 the expression of formerly downregulated hippocampal genes linked to cognition. In fact, our detailed  
11 analyses revealed that Vorinostat reinstated the expression of a specific gene cluster in which nearly every  
12 hub-gene was shown to be essential for memory function. Hence, reducing either of these genes alone  
13 was found to cause memory impairment (see supplemental table 3). While these findings are in line with  
14 the know role of Vorinostat to induced euchormatin and gene-expression, it was surprising to see that  
15 Vorinostat treated CamkII $\delta$  TG also exhibited reduced expression of genes linked to cellular stress  
16 responses. Our data suggest that this effect is mediated via the induction of a compensatory microRNA  
17 network that downregulated cellular stress response hub genes (**Fig 6**). These findings are in line with the  
18 reported role of the microRNAome as one key molecular process to maintain cellular homeostasis and  
19 reports that link microRNA expression to compensatory mechanisms in various diseases (Gebert &  
20 MacRae, 2019). We cannot exclude the possibility that the improved memory function in response to  
21 Vorinostat-treatment is mediated by other mechanisms. For example, Vorinsotat also acts on non-histone  
22 proteins and has been found to suppress hypoxia signaling in cancer models (Zhang, Yang et al., 2017).  
23 Moreover, although Vorinostat increases H3K4me3, this indirect effect is most likely mediated by  
24 increased histone acetylation that generally promotes euchromatin formation. In line with this previous  
25 findings show that Kmts act in concert with histone-acetyltransferases (Kerimoglu et al., 2013)  
26 (Kerimoglu et al., 2017) (Husmann & Gozani, 2019). Nevertheless, in the future, it will be important to  
27 investigate whether therapeutic approaches that target more directly H3K4me3 are even more efficient to  
28 reinstate memory function in response to HF.

29 In conclusion, our data elucidate the molecular mechanisms by which cardiac dysfunction contributes to  
30 cognitive impairment and suggest a key role for epigenetic neuronal gene expression. Targeting gene  
31 expression changes in the brain, through drugs such as HDAC inhibitor Vorinostat, ameliorate memory  
32 impairment and partially reinstate physiological gene expression. Thus, therapeutic strategies that target  
33 epigenetic gene expression may be a suitable approach to treat cognitive dysfunction even in chronic  
34 heart failure patients and lower their risk of developing age-associated cognitive diseases such as AD.

1

## 2 **Material and Methods**

3 More detailed information is available as a supplementary material & methods file.

4

### 5 *Animals and tissue preparation*

6 CamkII $\delta$ c transgenic and wild type littermates were housed in standard cages on 12h/12h light/dark cycle  
7 with food and water ad libitum. All experimental protocols were approved by a local animal care  
8 protocol. Unless otherwise stated, 3-month old mice were used for the experiments. For tissue  
9 preparation animals were sacrificed by cervical dislocation. Hippocampal sub-region CA1 was isolated,  
10 snap frozen in liquid nitrogen and stored at -80 °C. Hearts were dissected by a cut above the base of the  
11 aorta and perfused with 0.9% sodium chloride solution until blood free, snap frozen in liquid nitrogen and  
12 stored at -80°C. In addition, lung and tibia were extracted and their respective weight or length was  
13 determined.

14

### 15 *Echocardiography*

16 The heart function and dimensions were examined by echocardiography using a Vevo 2100 imaging  
17 platform (Visualsonics) with 30MHz transducer (MS-400). The animals were anesthetized with isoflurane  
18 (1-2%) and M-mode sequences of the beating heart recorded in the short-axis and the long axis,  
19 respectively. The images were used to determine the left ventricular end-diastolic and end-systolic  
20 Volumes (area\*length\*5/6). These parameters were used to calculate the ejection fraction as indicator of  
21 left ventricular heart function. The investigator was blinded to genotype and age.

22

### 23 *Behavioural tests and data analysis*

#### 24 *Open Field & Barnes Maze*

25 Open field test was performed according to a previous study (Bahari-Javan, Maddalena et al., 2012).  
26 Briefly, mice were placed gently in the middle quadrant of an open field and allowed to explore the arena  
27 for 5 minutes. The travel trajectories were recorded using VideoMot (TSE-Systems). Barnes Maze  
28 experiment was performed according to Sunyer et al (Sunyer, Patil et al., 2007).

29

#### 30 *RNA isolation and sequencing*

31 RNA isolation was performed using RNA Clean and Concentrator kit according to manufacturer protocol  
32 without modifications. Concentration was measured on nanodrop and quality of RNA was evaluated. For  
33 mRNA sequencing, 500 ng total RNA was used as input to prepare cDNA libraries according to Illumina  
34 Truseq and 50 bp sequencing reads were run in HiSeq 2000. For small RNA sequencing, 100 ng total

1 RNA was used as initial input. Small RNA was enriched using size selection from based on gel. cDNA  
2 library and sequencing have been performed according to manufacturer's protocol (NEBNext Small RNA  
3 library prep set for Illumina). Next generation sequencing was performed on HiSeq 2000 platform.

4

#### 5 *Chromatin immunoprecipitation for H3K4me3*

6 Chromatin immunoprecipitation was performed according to (Halder et al., 2016) with 0.2 µg chromatin  
7 and 1µg H3K4me3 (ab8580) antibody. ChIPseq library preparation was performed using NEBNext Ultra  
8 II DNA library preparation according to manufacturer's protocol. 2nM libraries were pooled and  
9 sequenced in Illumina Hiseq 2000 with 50-bp single end reads. Details are given in Supplementary File.

10

#### 11 *Modeling hypoxia and endoplasmic reticulum stress in primary neurons*

12 Primary hippocampal neuronal culture was prepared as described previous (Benito et al., 2015)  
13 Experiments were performed at DIV 10. Endoplasmic reticulum stress was induced in primary  
14 hippocampal neurons using Tunicamycin (Sigma Aldrich). 2ug/mL of Tunicamycin was added to primary  
15 neuronal culture and incubated for 6 hours and compared to those treated with DMSO for same time. To  
16 model hypoxia, primary hippocampal neuronal cultures were incubated in normoxia (20% O<sub>2</sub>) in a  
17 standard cell culture incubator for 10 days before they were used in an experiment. For hypoxic  
18 conditions cells were incubated at 1% O<sub>2</sub> for 4 hours using the *in vivo*<sub>2</sub> 400 hypoxia workstation (Baker  
19 Ruskin). Cells from the same isolation were kept in normoxia at 20% O<sub>2</sub> as a control.

20

#### 21 *Quantitative RT-PCR*

22 qPCR (q-PCR) primers were designed using Universal probe library Assay Design Center and were  
23 purchased from Sigma. Transcriptor High Fidelity cDNA Synthesis Kit (Roche) was used to prepare  
24 cDNA. UPL probes were used for quantification and data was normalized to HPRT1 expression as  
25 internal control. Relative gene expression was analyzed by 2-ddCt method. Primer sequences are  
26 summarized in Supplementary File.

27

#### 28 *Western blot*

29 Western blot was performed according to previous study (Bahari-Javan et al., 2012). To quantify  
30 H3K4me3 and H3K9ac levels H3K4me3 (abcam, ab8580) antibody, H3K9ac (abcam, ab4441) antibody  
31 were used respectively. Unmodified H3 level measured with H3 antibody (abcam, ab1791) was used as  
32 internal control.

33

#### 34 *Bioinformatics analysis*

1 Bulk RNA Sequencing data analysis has been performed according to (Benito et al., 2015). Small RNA  
2 sequencing files were analyzed according to using miRDeep2. A wrapper of the steps applied during  
3 mapping and counting is available as package (<https://github.com/mdrezaulislam/MicroRNA>).  
4 Differentially expressed genes or microRNAs were determined using mixed linear model accounting for  
5 technical and biological covariates.  
6 For linear mixed effects model, limma in R was implemented. Biological processes were analyzed using  
7 Gene Ontology (<http://geneontology.org/>). For pathway analysis KEGG (<https://www.genome.jp/kegg/>),  
8 Reactome (<https://reactome.org/>) databases were used. Exon counts were generated using DEXSeq  
9 (<http://bioconductor.org/packages/DEXSeq/>). Hypergeometric test analysis was performed using  
10 GeneOverlap (<http://bioconductor.org/packages/GeneOverlap/>). H3K4me3 peaks were called using  
11 MACS2. Chip peaks were mapped at promoter (TSS  $\pm$  2kb) of genes using ngs.plot. Weighted co-  
12 expression analysis for both microRNAs and mRNAs was performed using WGCNA (Langfelder &  
13 Horvath, 2008). External gene expression datasets that have been used from other studies were  
14 downloaded from NCBI GEO (<https://www.ncbi.nlm.nih.gov/geo/>) and mapped in house to have  
15 consistency in results. Details of microRNA promoter and host genes and other analysis are summarized  
16 in Supplementary File.

17

### 18 *Statistical analysis*

19 All the statistical analyses as mentioned in the main text are performed in Prism (version 7.0) or in R.

20

### 21 *Accession number for RNA-seq and ChIP-seq data*

22 Raw data for all next-generation sequencing samples can be accesses via the following accession number  
23 via GEO database: RNA-seq (GEO\*), smallRNA-seq (GEO\*), ChIP-seq (GEO\*)

24 \*will be made available upon acceptance of the manuscript.

25

### 26 **Acknowledgments**

27 The authors thank Susanne Burkhard, Alessya Kretzschmar and Sabrina Koszewa for technical support.

28 This work was supported by the funds from the SFB1002 (D04) of the German Research Foundation  
29 (DFG) to KT, DMK was supported by funds from the IRTG1816 and DFG Ka1269/13-1 of ther DFG. AF  
30 was supported by the DZNE, the DFG under Germany's Excellence Strategy - EXC 2067/1 390729940  
31 and the Hans and Ilse Breuer Foundation.

32

### 33 **Authors contribution**

1 MRI coordinated the project, performed experiment, analyzed data, and wrote the manuscript. DL breed  
2 mice and performed echo, MSS performed ChIP-seq, RMH contributed to some behavioral experiments  
3 and echo analysis; TB performed tissue dissection, MSS performed qPCR analysis, JC performed  
4 immunoblot analysis, EV contributed to the analysis of Barnes Maze data, CS, DMK and AZ performed  
5 hypoxia experiments, FS, KT, AF designed the project, KT and AF wrote the manuscript and co-  
6 supervised all work related to this manuscript.

7  
8

### 9 **Conflict of Interest**

10 The authors declare no competing financial interest

11

### 12 **Figure Legends.**

#### 13 **Fig. 1: Heart failure in CamkII $\delta$ TG mice is linked to aberrant hippocampal gene-expression. A.**

14 qPCR data showing expression of the CamkII $\delta$  in the brain and heart of 3 month old CamkII $\delta$  TG mice;  
15 n=4/group; \**P* <0.05). **B.** Representative M-mode images from left ventricle from CamkII $\delta$  TG and  
16 control mice. ESD: Left ventricle end systolic diameter, EDD: Left ventricle diastolic diameter. **C.** Left  
17 panel: Ejection fraction is significantly decreased in CamkII $\delta$  TG mice (n =8) when compared to control  
18 mice (n=5; \**P* <0.05). Heart weight (middle panel) and left ventricle weight (right panel) are increased in  
19 CamkII $\delta$  TG (n=8) compared to control (n=5; \**P* <0.05). **D.** Experimental scheme for RNA-seq analysis  
20 that was performed from hippocampal CA1 region of CamkII $\delta$  TG mice (n=6) and control mice (n=5) at  
21 3 month of age. Right panel shows principle component analysis (PCA) of the gene-expression data. The  
22 first principle component (PC1) can explain 42  
23 % of the variation between two groups. **E.** Volcano plot showing differentially expressed genes  
24 (FDR<0.05). Red color indicates up-regulation while blue represents down-regulation of transcripts. **F.**  
25 Hypergeometric overlap analysis comparing genes deregulated in CamkII $\delta$  TG mice to genes uniquely  
26 expressed in neurons, astrocytes or microglia. **G.** Dot plot showing Top GO biological processes after  
27 removing redundant GO terms using Rivago. **H.** qPCR quantification of selected genes reflecting ER-  
28 stress or protein methylation-related processes (n = 5/group) \**p*<0.05, Unpaired t-test; two-tailed Data is  
29 normalized to Hprt1 expression. **I.** Hypergeometric overlap analysis comparing genes deregulated in  
30 CamkII $\delta$  TG mice to genes deregulated under hypoxia conditions and in response to tunicamycin-  
31 induced ER-stress **J.** Hypergeometric overlap analysis comparing genes deregulated in CamkII $\delta$  TG  
32 mice to genes deregulated in hippocampal tissue from animal models of memory impairment and  
33 neurodegeneration. \**p*<0.05, \*\**p*<0.01, \*\*\**p*<0.001 Unpaired t-test; two-tailed. Error bars indicate SEM.

34



1 **Fig. 2: CamkII $\delta$ c TG mice display impaired hippocampus-dependent memory function.** A. The  
2 distance traveled (left panel), the speed (middle panel) and the time spent in the center region (right panel)  
3 during a 5 min open field test was similar amongst 3 months old CamkII $\delta$ c TG (n = 16) and control mice  
4 (n = 13). B. The time to enter the escape hole during training sessions of the Barnes maze test is impaired  
5 in old CamkII $\delta$ c TG (n = 16) and control mice (n = 13; two-way ANOVA, \*p<0.05). C. Plots showing  
6 the different search strategies of CamkII $\delta$ c TG (n = 16) and control mice (n = 13) across training trials.  
7 Each strategy is labeled with a unique color. D. The cumulative score of hippocampus-dependent search  
8 strategies during Barnes maze training is impaired in CamkII $\delta$ c TG (n = 16) when compared to control  
9 mice (n = 13; two-tailed, unpaired t-test, \*p<0.05). E. Number of visits to escape hole during probe test to  
10 assay memory retrieval was impaired in CamkII $\delta$ c TG (n = 16) when compared to control mice (n = 13;  
11 two-tailed, unpaired t-test, \*p<0.05). Error bar indicates mean  $\pm$  SEM.

12  
13 **Fig. 3: Neuronal H3K4m3 is impaired in the hippocampus of CamkII $\delta$ c TG mice** A. Hypergeometric  
14 overlap analysis comparing genes deregulated in CamkII $\delta$ c TG mice to genes differentially expressed in  
15 the hippocampal CA1 region of Kat2A, Kmt2A and Kmt2b knock out mice. B. Experimental scheme for  
16 Chip-seq analysis. C. Pie chart showing the distribution of H3K4me3 peaks in the neurons of the  
17 hippocampal CA1 region from CamkII $\delta$ c TG mice. D. MA plot showing the number of significantly  
18 altered neuronal H3K4me3 peaks when comparing CamkII $\delta$ c TG and control mice. E. NGS plot showing  
19 H3K4me3 peaks at the TSS of genes down-regulated in the hippocampus of CamkII $\delta$ c TG mice. Inset  
20 shows statistical analysis, (\*\*\*)P < 0.001). Error bars indicate SEM.

21  
22 **Fig. 4: Vorinostat reinstates memory function in CamkII $\delta$ c TG mice.** A Schematic outline of the  
23 experimental design. B. The distance traveled (upper panel), the speed (middle panel) and the time spent  
24 in the center region (lower panel) during a 5 min open field test were similar amongst groups  
25 (n=10/group). C. Latency to enter the escape hole during Barnes maze training (Two-way ANOVA,  
26 \*\*p<0.01). D. Plots showing the different search strategies across training trials. Each strategy is labeled  
27 with a unique color. E. Cumulative hippocampus-dependent strategy scores during the Barnes maze  
28 training (One-way ANOVA, \*p<0.05). F. Number of visits to the escape hole during probe test  
29 (\*\*p<0.01). Error bars indicate mean  $\pm$  SEM.

30  
31 **Fig. 5: Vorinostat ameliorates pathological hippocampal gene-expression in CamkII $\delta$ c TG mice.** A.  
32 Schematic outline of the experimental design. B. Scheme for WGCNA analysis. C. Upper panel:  
33 Expression of RNA module 1 among the three experimental groups. \*p<0.05, Kruskal-Wallis test Lower  
34 panel: Gene ontology analysis of genes that are part of RNA module 1. D. Network representing top 30  
35 hub genes of the gene network based on RNA module 1. E. Upper panel: RNA module 2 and its

1 expression among the three experimental groups \* $p < 0.05$ , Kruskal-wallis test. Lower panel: Functional  
2 annotations of the genes that are part of RNA module 2. **F.** Gene correlation network of the top hub genes  
3 ( $n = 30$ ) of RNA module 2. **G.** Left panel: Schematic outline of the analysis of microRNA-sequencing  
4 data. Right panel: Expression of microRNA module 2 amongst experimental groups. Kruskal-Wallis test.  
5 \*\* $p < 0.01$ . **H.** Heatmap showing significant negative correlation ( $FDR < 0.05$ ) between microRNA  
6 members of microRNA module 2 and hub genes from RNA module 2 (see Fig 5E). Error bars indicate  
7 SEM.

8

9 **Fig. 6. Model summarizes how heart failure contributes to memory impairment and corresponding**  
10 **option for therapeutic intervention.** Cardiac insufficiency leads to cerebral hypoperfusion, which is in  
11 line with a hippocampal gene-expression response linked to oxidative, and ER-stress. Our data suggest  
12 that oxidative and ER-stress drive reduced expression of genes important for memory function, which  
13 involves reduced neuronal H3K4me3 representation loss of euchromatin. Administration of the HDAC  
14 inhibitor Vorinostat partially increases the expression of memory-related genes but also decreases the  
15 expression of genes linked to oxidative and ER-stress via the induction of a microRNA cluster.

16

17 **Expanded view Fig 1. Vorinostat increases H3K4me3 level in primary neurons.** Primary mouse  
18 hippocampal neuronal cultures (10 DIV;  $n=3$ /group) were treated for 1h with Vorinostat ( $1\mu\text{m}$ ) or vehicle  
19 before proteins were isolated and subjected to immunoblot analysis. Left panel: Representative  
20 immunoblot analysis. H3 was used as loading control. Right panels: Semi-quantitative analysis of  
21 immunoblot analysis from two independent experiments ( $n=3$ /group and experiment). Relative Intensity  
22 was normalized to H3 level. The data reveal that Vorinostat treatment significantly increases bulk levels  
23 of H3K4me3 and H3K9ac. \* $P < 0.05$ , t-test; Error bars indicate SEM.

24

25 **Expanded View Fig 2: Cardiac function is not significantly affected in CamkII $\delta$ c TG mice upon**  
26 **Vorinostat treatment.** **A.** Scheme of the experimental design. Vorinostat treat was initiated at 2 month  
27 of age and analysis was performed at 3 month of age.  $n = 10$ /group. **B.** Violin plot showing that body  
28 weight was similar amongst groups. **C.** Violin plots showing that heart weight and left ventricle (LV)  
29 weight (**D**) was increased in vehicle and Vorinostat-treated CamkII $\delta$ c TG mice when compared to the  
30 wild-type vehicle control group. ns; not significant, \* $P < 0.05$ , \*\* $P < 0.01$ , \*\*\*  $P < 0.001$ , Kruskal wallis  
31 t-Test.

32

33 **Expanded View Fig 3: Weighted gene co-expression analysis upon Vorinostat treatment.** **A.** Volcano  
34 plot showing significantly deregulated genes in the hippocampal CA1 region, when comparing vehicle-

1 treated CamkII $\delta$ c Tg mice to vehicle-treated control mice (FDR < 0.05). Up- and down-regulated genes  
2 are represented in darkred and darkblue colors respectively. **B.** Pathways affected in the hippocampal  
3 CA1 region when comparing vehicle-treated wild type vs. CamkII $\delta$ c mice to Vorinostat-treated CamkII $\delta$ c  
4 vs vehicle-treated wild type mice. Note that Vorinostat-treatment ameliorates pathways affected in  
5 CamkII $\delta$ c TG mice for pathway increased and decreased under pathological conditions. **C.** Venn diagram  
6 showing common and uniquely deregulated genes between groups. **D.** Soft power selection based on  
7 scale independence and mean connectivity for different modules identification in WGCNA. **E.** Different  
8 modules representing distinct expression patterns among groups. Y axis representing eigen expression of  
9 given cluster/module.

10

11 **Expanded View Fig. 4: Hypogeometric overlap analysis comparing conserved the gene-expression**  
12 **networks RNA module 1 and 2 to hypoxic and ER stress conditions.**

13 Heatmaps summarizing results from hypergeometric tests for genes in RNA module 1 and 2 with stress  
14 conditions in different experimental settings. Hypoxia (1% O<sub>2</sub>, 4h) and endoplasmic stress (tunicamycin  
15 2 ug/mL, 6h) was modeled in primary hippocampal neurons. Gene expression data on hypoxia from  
16 human brain organoid data is retrieved from Pasca et al, 2019. Up and down regulated genes (FDR<0.05)  
17 were determined by comparing to corresponding controls. Enrichment significance cutoff: FDR < 0.05.  
18 Color intensity represents fold enrichment.

19

20 **Expanded View Fig 5. Vorinostat induced microRNA expression changes in the hippocampal CA1**

21 **region of CamkII $\delta$ c TG mice. A.** Volcano plot showing differentially expressed microRNAs when  
22 comparing Vorinostat-treated to vehicle treated CamkII $\delta$ c TG mice. **B.** Expression of microRNA modules  
23 from WGCNA analysis in three experimental groups. wild type vehicle: n = 9; CamkII $\delta$ c TG-vehicle n =  
24 7; CamkII $\delta$ c TG-Vorinostat n = 10; kruskal wallis test. **C.** H3K4me3 profile at promoter of genes that  
25 harbor microRNAs. H3K4me3 level at promoter of these genes is significantly reduced in transgenic mice.  
26 Unpaired t -test , \*p<0.05 . Error bars indicate SEM.

27

28 **Literature**

29 Ampadu J, Morley JE (2015) Heart failure and cognitive dysfunction. *Int J Cardiol* 15: 12-23  
30 Angermann CE, Frey A, Ertl G (2012) Cognition matters in cardiovascular disease and heart  
31 failure. *Eur Heart J* 33: 1721-1723  
32 Arnold JM, Liu P, Demers C, Dorian P, Giannetti N, Haddad H, Heckman GA, Howlett JG,  
33 Ignaszewski A, Johnstone DE, Jong P, McKelvie RS, Moe GW, Parker JD, Rao V, Ross HJ, Sequeira  
34 EJ, Svendsen AM, Teo K, Tsuyuki RT et al. (2006) Canadian Cardiovascular Society. Canadian

- 1 Cardiovascular Society consensus conference recommendations on heart failure 2006:  
2 diagnosis and management. *Can J Cardiol* 22: 23-45
- 3 Bahari-Javan S, Maddalena A, Kerimoglu C, Wittnam J, Held T, Bähr M, Burkhardt S, Delalle I,  
4 Kügler S, Fischer A, Sananbenesi F (2012) HDAC1 Regulates Fear Extinction in Mice. *J Neurosci*  
5 32: 5062-5073
- 6 Bahari-Javan S, Varbanov H, Halder R, Benito E, Kaurani L, Burkhardt S, Anderson-Schmidt H,  
7 Angheliescu I, Budde M, Stilling RM, Costa J, D. D, Figge C, Folkerts H, Gade K, Heilbronner U,  
8 Koller M, Konrad C, Nussbeck SY, Scherk H et al. (2017) HDAC1 LINKS EARLY LIFE STRESS TO  
9 SCHIZOPHRENIA-LIKE PHENOTYPES. *Proc Natl Acad Sci U S A* 114: E4686-E4694
- 10 Benito E, Urbanke E, Barth J, Halder R, Capece V, Jain G, Burkhardt S, Navarro M, Schutz AL,  
11 Bonn S, Fischer A (2015) Reinstating transcriptome plasticity and memory function in mouse  
12 models for cognitive decline. *J Clin Invest* 125: 3572-3584
- 13 Bikkina M, Levy D, Evans JC, Larson MG, Benjamin EJ, Wolf PA, Castelli WP (1994) Left  
14 ventricular mass and risk of stroke in an elderly cohort. The Framingham Heart Study. *JAMA*  
15 272: 33-36
- 16 Bjornsson HT, Benjamin JS, Zhang L, Weissman J, Gerber EE, Chen YC, Vaurio RG, Potter MC,  
17 Hansen KD, Dietz HC (2014) Histone deacetylase inhibition rescues structural and functional  
18 brain deficits in a mouse model of Kabuki syndrome. *Sci Transl Med* 6: 256ra135
- 19 Butterfield DA, Halliwell B (2019) Oxidative stress, dysfunctional glucose metabolism and  
20 Alzheimer disease. *Nat Rev Neurosci* 20: 148-160
- 21 Cermakova P, Lund LH, Fereshtehnejad SM, Johnell K, Winblad B, Dahlström U, Eriksson M,  
22 Religa D (2015) Heart failure and dementia: survival in relation to types of heart failure and  
23 different dementia disorders. *Eur J Heart Fail* 17: 612-619
- 24 Cleland JG, Daubert JC, Erdmann E, Freemantle N, Gras D, Kappenberger L, Tavazzi L,  
25 Investigators CR-HFC-HS (2005) The effect of cardiac resynchronization on morbidity and  
26 mortality in heart failure. *N Engl J Med* 352: 1539-1549
- 27 Doehner W, Ural D, Haessler KG, Čelutkienė J, Bestetti R, Cavusoglu Y, Peña-Duque MA, Glavas  
28 D, Iacoviello M, Laufs U, Alvear RM, Mbakwem A, Piepoli MF, Rosen SD, Tsivgoulis G, Vitale C,  
29 Yilmaz MB, Anker SD, Filippatos G, Seferovic P et al. (2017) Heart and brain interaction in  
30 patients with heart failure: overview and proposal for a taxonomy. A position paper from the  
31 Study Group on Heart and Brain Interaction of the Heart Failure Association. *Eur J Heart Fail* 20:  
32 199-215
- 33 Evonuk KS, Prabhu SD, Young ME, DeSilva TM (2017) Myocardial ischemia/reperfusion impairs  
34 neurogenesis and hippocampal-dependent learning and memory. *Brain Behav Immun* 61: 266-  
35 273
- 36 Feldstein CA (2012) Association between chronic blood pressure changes and development of  
37 Alzheimer's disease. *J Alzheimers Dis* 32: 753-763
- 38 Fischer A (2014a) Epigenetic memory: the Lamarckian brain. *EMBO J* 33: 945-967
- 39 Fischer A (2014b) Targeting histone-modifications in Alzheimer's disease. What is the evidence  
40 that this is a promising therapeutic avenue? *Neuropsychopharmacology* 80: 95-012
- 41 Frigerio M, Roubina E (2005) Drugs for left ventricular remodeling in heart failure. *Am J Cardiol*  
42 96: 10L-18L
- 43 Galli A, Lombardi F (2014) Neprilysin inhibition for heart failure. *N Engl J Med* 371: 2335

- 1 Gandal MJ, Zhang P, Hadjimichael E, Walker RL, Chen C, Liu S, Won H, van Bakel H, Varghese M,  
2 Wang Y, Shieh AW, Haney J, Parhami S, Belmont J, Kim M, Moran Losada P, Khan Z, Mleczko J,  
3 Xia Y, Dai R et al. (2018) Transcriptome-wide isoform-level dysregulation in ASD, schizophrenia,  
4 and bipolar disorder. *Science* 362: doi: 10.1126/science.aat8127
- 5 Gebert LFR, MacRae IJ (2019) Regulation of microRNA function in animals. *Nat Rev Mol Cell Biol*  
6 20: 21-37
- 7 Gispert S, Brehm N, Weil J, Seidel K, Rüb U, Kern B, Walter M, Roeper J, Auburger G (2015)  
8 Potentiation of neurotoxicity in double-mutant mice with Pink1 ablation and A53T-SNCA  
9 overexpression. *Hum Mol Genet* 24: 1061-1076
- 10 Gjoneska E, Pfenning AR, Mathys H, Quon G, Kundaje A, Tsai LH, Kellis M (2015) Conserved  
11 epigenomic signals in mice and humans reveal immune basis of Alzheimer's disease. *Nature*  
12 518: 365-369
- 13 Govindarajan N, Agis-Balboa C, Walter J, Sananbenesi F, Fischer A (2011) Sodium Butyrate  
14 Improves Memory Function in an Alzheimer's Disease Mouse Model When Administered at an  
15 Advanced Stage of Disease Progression. *Journal of Alzheimer's Disease* 24: 1-11
- 16 Gupta S, Kim SY, Artis S, Molfese DL, Schumacher A, Sweatt JD, Paylor RE, Lubin FD (2010)  
17 Histone methylation regulates memory formation. *J Neurosci* 30: 3589-3599
- 18 Gurtan AM, Sharp PA (2013) The Role of miRNAs in Regulating Gene Expression Networks. *J Mol*  
19 *Biol pii*: Epub ahead of print
- 20 Hajduk AM, Lemon SC, McManus DD, Lessard DM, Gurwitz JH, Spencer FA, Goldberg RJ,  
21 Saczynski JS (2013) Cognitive impairment and self-care in heart failure. *Clin Epidemiol* 24: 407-  
22 416
- 23 Halder R, Hennion M, Vidal RO, Shomroni O, Rahman RU, Rajput A, Centeno TP, van Bebber F,  
24 Capece V, Vizcaino JC, Schuetz AL, Burkhardt S, Benito E, Sala MN, Javan SB, Haass C, Schmid B,  
25 Fischer A, Bonn S (2016) DNA methylation changes in plasticity genes accompany the formation  
26 and maintenance of memory. *Nat Neurosci* 19: 102-110
- 27 Husmann D, Gozani O (2019) Histone lysine methyltransferases in biology and disease. *Nat*  
28 *Struct Mol Biol* 26: 880-889
- 29 Jakovcevski M, Ruan H, Shen EY, Dincer A, Javidfar B, Ma Q, Peter CJ, Cheung I, Mitchell AC,  
30 Jiang Y, Lin CL, Pothula V, Stewart AF, Ernst P, Yao WD, Akbarian S, Impey S (2015) Neuronal  
31 Kmt2a/Mll1 histone methyltransferase is essential for prefrontal synaptic plasticity and working  
32 memory. *J Neurosci* 35: 5097-5108
- 33 Kagias K, Nehammer C, Pockock R (2012) Neuronal responses to physiological stress. *Front Genet*  
34 3: eCollection 2012
- 35 Kerimoglu C, Agis-Balboa RC, Kranz A, Stilling R, Bahari-Javan S, Benito-Garagorri E, Halder R,  
36 Burkhardt S, Stewart AF, Fischer A (2013) Histone-methyltransferase mll2 (kmt2b) is required  
37 for memory formation in mice. *J Neurosci* 33: 3452-3464
- 38 Kerimoglu C, Sakib MS, Jain G, Benito E, Burkhardt S, Capece V, Kaurani L, Halder R, Agis-Balboa  
39 RC, Stilling R, Urbanke H, Kranz A, Stewart AF, Fischer A (2017) KMT2A and KMT2B Mediate  
40 Memory Function by Affecting Distinct Genomic Regions. *Cell reports* 20: 538-548
- 41 Khachaturian AS, Zandi PP, Lyketsos CG, Hayden KM, Skoog I, Norton MC, Tschanz JT, Mayer LS,  
42 Welsh-Bohmer KA, Breitner JC (2006) Antihypertensive medication use and incident Alzheimer  
43 disease: the Cache County Study. *Arch Neurol* 63: 686-692

1 Kilgore M, Miller CA, Fass DM, Hennig KM, Haggarty SJ, Sweatt JD, Rumbaugh G (2010)  
2 Inhibitors of class 1 histone deacetylases reverse contextual memory deficits in a mouse model  
3 of Alzheimer's disease. *Neuropsychopharmacology* 35: 870-880  
4 Kumar R, Woo MA, Macey PM, Fonarow GC, Hamilton MA, Harper RM (2011) Brain axonal and  
5 myelin evaluation in heart failure. *J Neurol Sci* 307-1-2  
6 Kumar R, Yadav SK, Palomares JA, Park B, Joshi SH, Ogren JA, Macey PM, Fonarow GC, Harper  
7 RM, Woo MA (2015) Reduced regional brain cortical thickness in patients with heart failure.  
8 *PLoS One* 10: e0126595  
9 Langfelder P, Horvath S (2008) WGCNA: an R package for weighted correlation network  
10 analysis. *BMC Bioinformatics* 29: eCollection  
11 Maier LS, Zhang T, Chen L, DeSantiago J, Brown JH, Bers DM (2003) Transgenic CaMKII $\delta$ C  
12 overexpression uniquely alters cardiac myocyte Ca $^{2+}$  handling: reduced SR Ca $^{2+}$  load and  
13 activated SR Ca $^{2+}$  release. *Circ Res* 92: 904-911  
14 Merienne N, Meunier C, Schneider A, Seguin J, Nair SS, Rocher AB, Gras S, Keime C, Faull R,  
15 Pellerin L, Chatton JY, Neri C, Merienne K, Déglon N (2019) Cell-Type-Specific Gene Expression  
16 Profiling in Adult Mouse Brain Reveals Normal and Disease-State Signatures. *Cell Rep* 26: 2477-  
17 2493  
18 Nestler EJ, Peña CJ, Kundakovic M, Mitchell A, Akbarian S (2015) Epigenetic Basis of Mental  
19 Illness. *Neuroscientist* 8  
20 Pan A, Kumar R, Macey PM, Fonarow GC, Harper RM, Woo MA (2013) Visual assessment of  
21 brain magnetic resonance imaging detects injury to cognitive regulatory sites in patients with  
22 heart failure. *J Card Fail* 19: 94-100  
23 Paşca AM, Park JY, Shin HW, Qi Q, Revah O, Krasnoff R, O'Hara R, Willsey AJ, Palmer TD, Paşca  
24 SP (2019) Human 3D cellular model of hypoxic brain injury of prematurity. *Nat Med* 25: 784-  
25 791  
26 Patel A, Moalem A, Cheng HB, abadjouni RM, Patel K, Hodis DM, Chandegara D, Cen S, He S, Liu  
27 Q, Mack WJ (2017) Chronic cerebral hypoperfusion induced by bilateral carotid artery stenosis  
28 causes selective recognition impairment in adult mice. *Neurol Res* 39: 910-917  
29 Peleg S, Sananbenesi F, Zovoilis A, Burkhardt S, Bahari-Java S, Agis-Balboa RC, Cota P, Wittnam  
30 J, Gogul-Doering A, Opitz L, Salinas-Riester G, Dettenhofer M, KAng H, Farinelli L, Chen W,  
31 Fischer A (2010) Altered histone acetylation is associated with age-dependent memory  
32 impairment in mice. *Science* 328: 753-756  
33 Perlman JM (2007) Pathogenesis of hypoxic-ischemic brain injury. *Journal of Perinatology* 27:  
34 39-47  
35 Ponikowski P, Voors AA, Anker SD, Bueno H, Cleland JGF, Coats AJS, Falk V, González-Juanatey  
36 JR, Harjola VP, Jankowska EA, Jessup M, Linde C, Nihoyannopoulos P, Parissis JT, Pieske B, Riley  
37 JP, Rosano GMC, Ruilope LM, Ruschitzka F, Rutten FH et al. (2018) ESC Scientific Document  
38 Group. 2016 ESC Guidelines for the diagnosis and treatment of acute and chronic heart failure:  
39 The Task Force for the diagnosis and treatment of acute and chronic heart failure of the  
40 European Society of Cardiology (ESC)Developed with the special contribution of the Heart  
41 Failure Association (HFA) of the ESC. *Eur Heart J* 37: 2129-2200  
42 Pressler SJ, Subramanian U, Kareken D, Perkins SM, Gradus-Pizlo I, Sauvé MJ, Ding Y, Kim J,  
43 Sloan R, Jaynes H, Shaw RM (2010) Cognitive deficits in chronic heart failure. *Nurs Res* 59: 127-  
44 139

- 1 Roy B, Woo MA, Wang DJJ, Fonarow GC, Harper RM, Kumar R (2017) Reduced regional cerebral  
2 blood flow in patients with heart failure. *Eur J Heart Fail* 19: 1294-1302
- 3 Satizabal CL, Beiser AS, Chouraki V, Chêne G, Dufouil C, Seshadri S (2016) Incidence of Dementia  
4 over Three Decades in the Framingham Heart Study. *N Engl J Med* 374: 523-532
- 5 Savarese G, Lund LH (2017) Global public health burden of heart failure. . *Cardiac failure review*  
6 3: 7-11
- 7 Solomon SD, Rizkala AR, Gong J, Wang W, Anand IS, Ge J, Lam CSP, Maggioni AP, Martinez F,  
8 Packer M, Pfeffer MA, Pieske B, Redfield MM, Rouleau JL, Van Veldhuisen DJ, Zannad F, Zile MR,  
9 Desai AS, Shi VC, Lefkowitz MP et al. (2017) Angiotensin Receptor Neprilysin Inhibition in Heart  
10 Failure With Preserved Ejection Fraction: Rationale and Design of the PARAGON-HF Trial. *JACC*  
11 *Heart Fail* 5: 471-482
- 12 Stilling R, Rönicke R, Benito-Garagorri E, Urbanke H, Capece V, Burckhard S, Bahari-Javan S,  
13 Barth J, Sananbenesi F, Schütz AL, Dyczkowski J, Martinez-Hernandez A, Kerimoglu C, Dent SR,  
14 Bonn S, Reymann KG, Fischer A (2014) K-Lysine acetyltransferase 2A regulates a hippocampal  
15 gene-expression network linked to memory formation. *EMBO J* 33: 1912-1927
- 16 Sunyer B, Patil S, Höger H, Lubec G (2007) Barnes maze, a useful task to assess spatial reference  
17 memory in the mice. *Nat Protoc* 390: 10-38
- 18 Swarup V, Hinz FI, Rexach JE, Noguchi KI, Toyoshiba H, Oda A, Hirai K, Sarkar A, Seyfried NT,  
19 Cheng C, Haggarty SJ, Consortium IFDG, Grossman M, Van Deerlin VM, Trojanowski JQ, Lah JJ,  
20 Levey AI, Kondou S, Geschwind DH (2018) Identification of evolutionarily conserved gene  
21 networks mediating neurodegenerative dementia. *Nat Med* 25: 152-164
- 22 Verdecchia P, Porcellati C, Reboldi G, Gattobigio R, Borgioni C, Pearson TA, G. A (2001) Left  
23 ventricular hypertrophy as an independent predictor of acute cerebrovascular events in  
24 essential hypertension. *Circulation* 104: 2039-2044
- 25 Wendeln AC DK, Kaurani L, Gertig M, Ulas T, Jain G, Wagner J,, Häslér LM WK, Skodras A, Blank  
26 T, Staszewski O, Datta M, Centeno TP, Capece , V IM, Kerimoglu C, Staufienbiel M, Schultze JL,  
27 Beyer M, Prinz M, Jucker M,, Fischer A NJ (2018) Innate immune memory in the brain shapes  
28 neurological disease hallmarks. *Nature* Epub ahead of print
- 29 Woo MA, Ogren JA, Abouzeid CM, Macey PM, Sairafian KG, Saharan PS, Thompson PM,  
30 Fonarow GC, Hamilton MA, Harper RM, Kumar R (2015) Regional hippocampal damage in heart  
31 failure. *Eur J Heart Fail* 17: 494-500
- 32 Xiang C, Wang Y, Zhang H, Han F (2017) The role of endoplasmic reticulum stress in  
33 neurodegenerative disease. *Apoptosis* 22: 1-26
- 34 Zhang C, Yang C, Feldman MJ, Wang H, Pang Y, Maggio DM, Zhu D, Nesvick CL, Dmitriev P,  
35 Bullova P, Chittiboina P, Brady RO, Pacak K, Zhuang Z (2017) Vorinostat suppresses hypoxia  
36 signaling by modulating nuclear translocation of hypoxia inducible factor 1 alpha. . *Oncotarget*  
37 8: 56110-56125
- 38

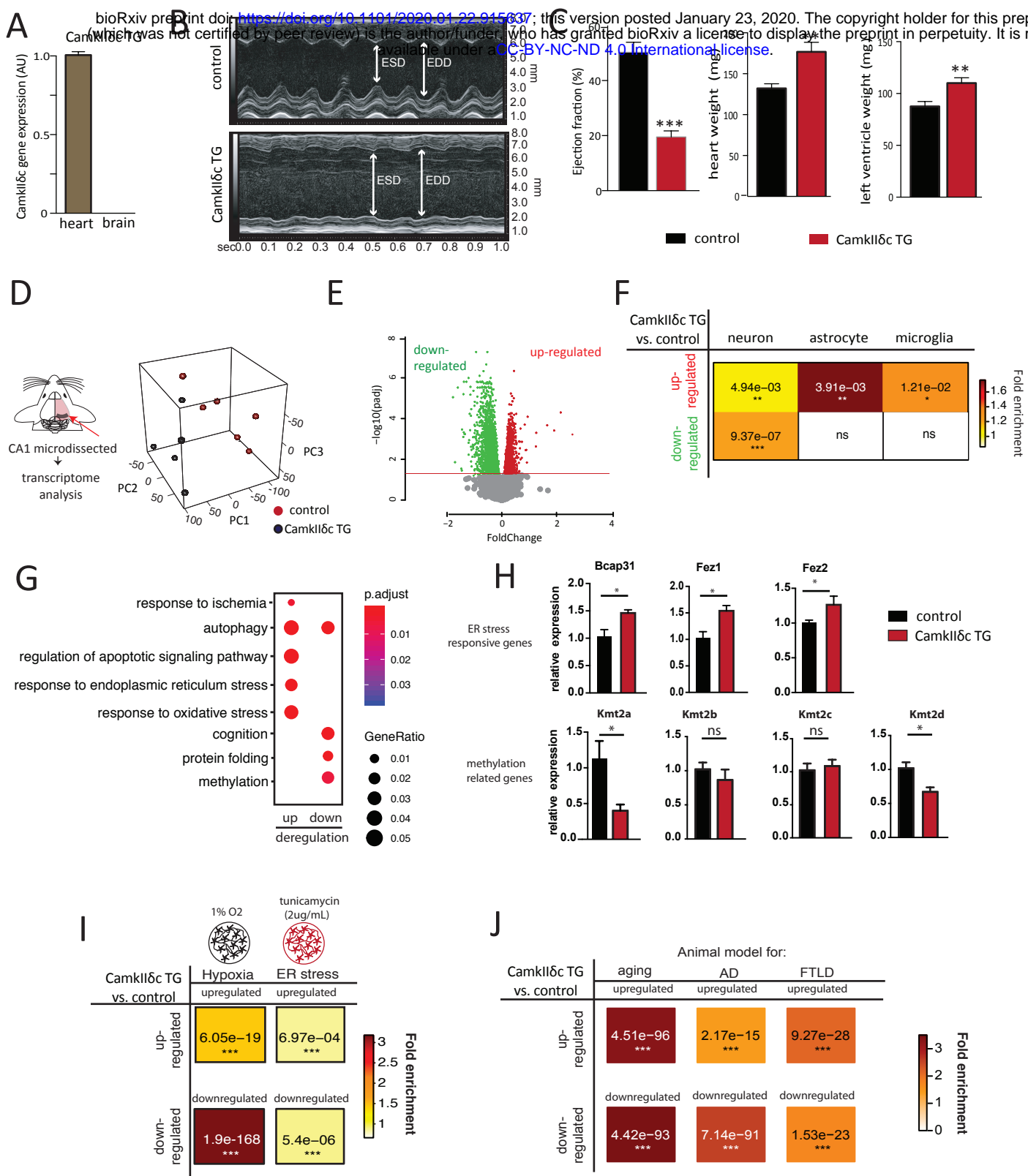


**Fig. 1: Heart failure in CamkIIδc TG mice is linked to aberrant hippocampal gene-expression.**

**A.** qPCR data showing expression of the CamkIIδc in the brain and heart of 3 month old CamkIIδc TG mice; n=4/group; \*P <0.05). **B.** Representative M-mode images from left ventricle from CamkIIδc TG and control mice. ESD: Left ventricle end systolic diameter, EDD: Left ventricle diastolic diameter. **C.** Left panel: Ejection fraction is significantly decreased in CamkIIδc TG mice (n=8) when compared to control mice (n=5; \*P <0.05). Heart weight (middle panel) and left ventricle weight (right panel) are increased in CamkIIδc TG (n=8) compared to control (n=5; \*P <0.05). **D.** Experimental scheme for RNA-seq analysis that was performed from hippocampal CA1 region of CamkIIδc TG mice (n=6) and control mice (n=5) at 3 month of age. Right panel shows principle component analysis (PCA) of the gene-expression data. The first principle component (PC1) can explain 42% of the variation between two groups. **E.** Volcano plot showing differentially expressed genes (FDR<0.05). Red color indicates upregulation while blue represents downregulation of transcripts. **F.** Hypergeometric overlap analysis comparing genes deregulated in CamkIIδc TG mice to genes uniquely expressed in neurons, astrocytes or microglia. **G.** Dot plot showing Top GO biological processes after removing redundant GO terms using Rivago. **H.** qPCR quantification of selected genes reflecting ER-stress or protein methylation-related processes (n = 5/group) \*p<0.05, Unpaired t-test; two-tailed Data is normalized to Hprt1 expression. **I.** Hypergeometric overlap analysis comparing genes deregulated in CamkIIδc TG mice to genes deregulated under hypoxia conditions and in response to tunicamycin-induced ER-stress **J.** Hypergeometric overlap analysis comparing genes deregulated in CamkIIδc TG mice to genes deregulated in hippocampal tissue from animal models of memory impairment and neurodegeneration. \*p<0.05, \*\*p<0.01, \*\*\*p<0.001 Unpaired t-test; two-tailed. Error bars indicate SEM.



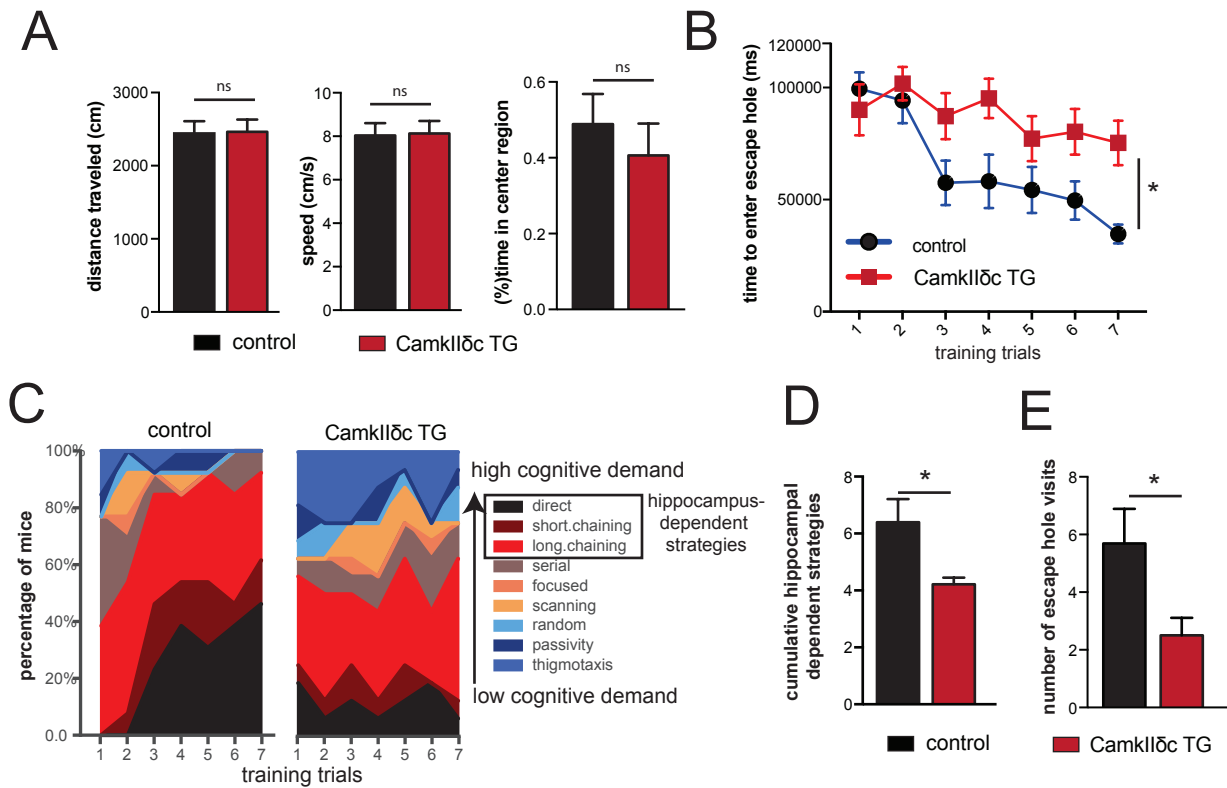


**Fig. 2: CamkIIδc TG mice display impaired hippocampus-dependent memory function.**

A. The distance traveled (left panel), the speed (middle panel) and the time spent in the center region (right panel) during a 5 min open field test was similar amongst 3 months old CamkIIδc TG ( $n = 16$ ) and control mice ( $n = 13$ ). B. The time to enter the escape hole during training sessions of the Barnes maze test is impaired in old CamkIIδc TG ( $n = 16$ ) and control mice ( $n = 13$ ; two-way ANOVA,  $*p < 0.05$ ). C. Plots showing the different search strategies of CamkIIδc TG ( $n = 16$ ) and control mice ( $n = 13$ ) across training trials. Each strategy is labeled with a unique color. D. The cumulative score of hippocampus-dependent search strategies during Barnes maze training is impaired in CamkIIδc TG ( $n = 16$ ) when compared to control mice ( $n = 13$ ; two-tailed, unpaired t-test,  $*p < 0.05$ ). E. Number of visits to escape hole during probe test to assay memory retrieval was impaired in CamkIIδc TG ( $n = 16$ ) when compared to control mice ( $n = 13$ ; two-tailed, unpaired t-test,  $*p < 0.05$ ). Error bar indicates mean  $\pm$  SEM.

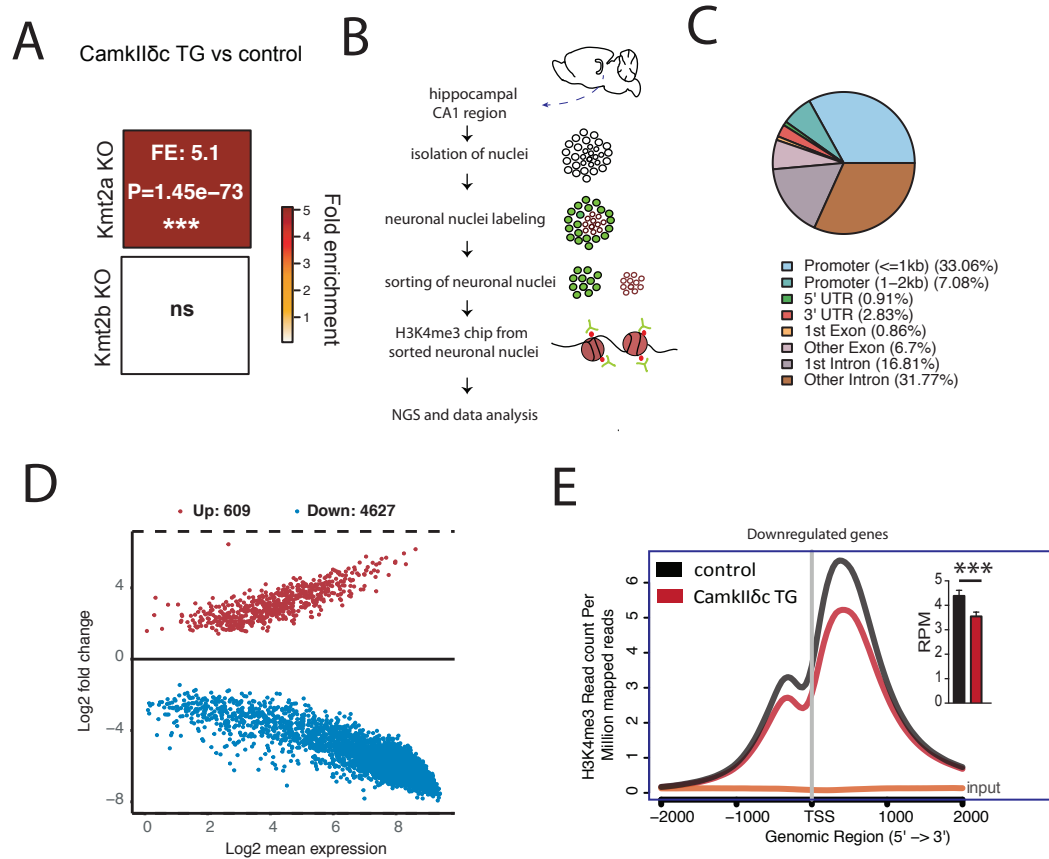


**Fig. 3: Neuronal H3K4m3 is impaired in the hippocampus of CamkII $\delta$ c TG mice**

A. Hypergeometric overlap analysis comparing genes deregulated in CamkII $\delta$ c TG mice to genes differentially expressed in the hippocampal CA1 region of Kat2A, Kmt2A and Kmt2b knock out mice. B. Experimental scheme for Chip-seq analysis. C. Pie chart showing the distribution of H3K4me3 peaks in the neurons of the hippocampal CA1 region from CamkII $\delta$ c TG mice. D. MA plot showing the number of significantly altered neuronal H3K4me3 peaks when comparing CamkII $\delta$ c TG and control mice. E. NGS plot showing H3K4me3 peaks at the TSS of genes down-regulated in the hippocampus of CamkII $\delta$ c TG mice. Inset shows statistical analysis, (\*\*\*)P < 0.001). Error bars indicate SEM.

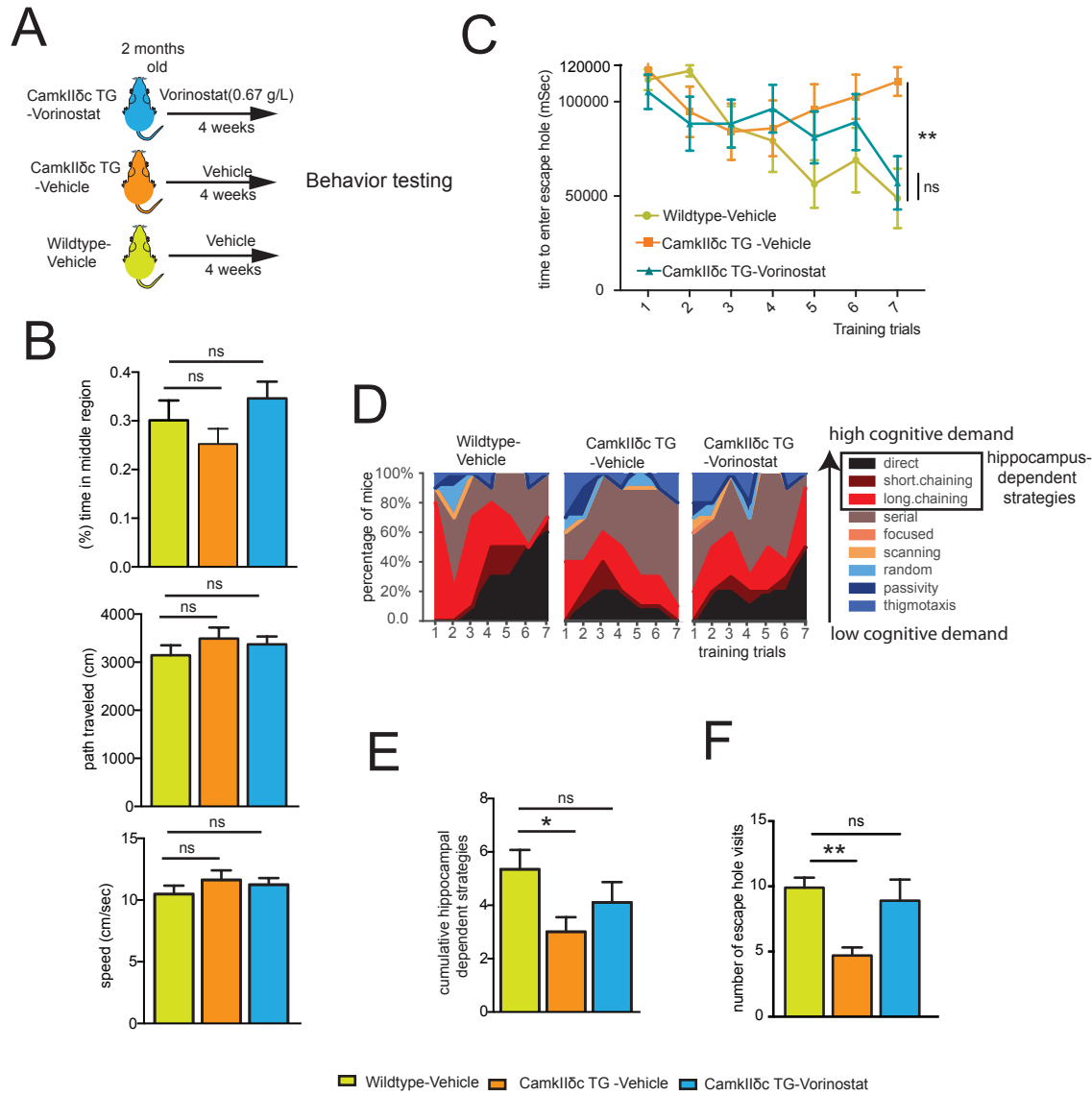


**Fig. 4: Vorinostat reinstates memory function in CamkIIδc TG mice.**

A Schematic outline of the experimental design. B. The distance traveled (upper panel), the speed (middle panel) and the time spent in the center region (lower panel) during a 5 min open field test was similar amongst groups ( $n=10/\text{group}$ ). C. Latency to enter the escape hole during Barnes maze training (Two-way ANOVA,  $**p<0.01$ ). D. Plots showing the different search strategies across training trials. Each strategy is labeled with a unique color. E. Cumulative hippocampus-dependent strategy scores during the Barnes maze training (One-way ANOVA,  $*p<0.05$ ). F. Number of visits to the escape hole during probe test ( $**p<0.01$ ). Error bars indicate mean  $\pm$  SEM.

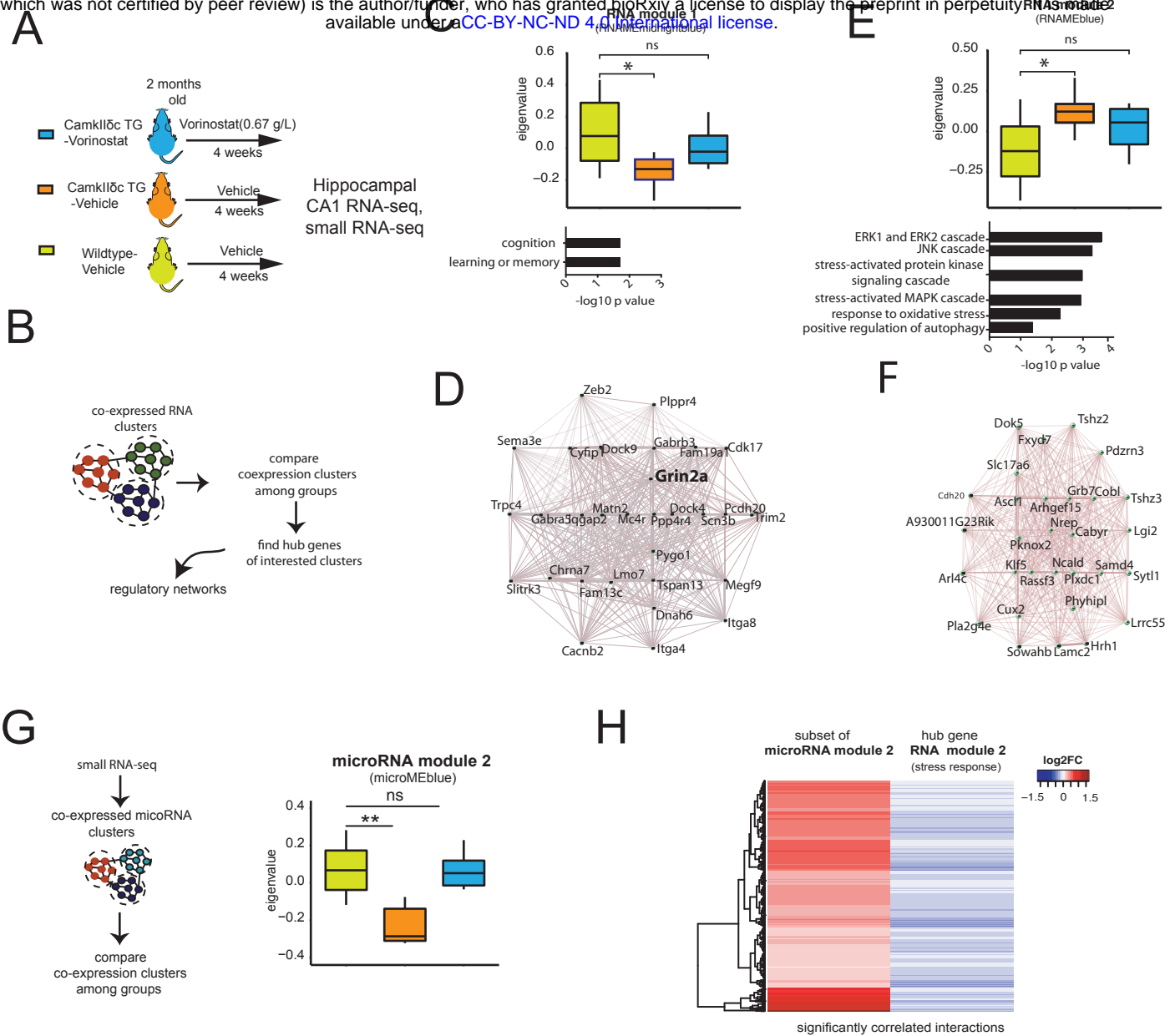


**Fig. 5: Vorinostat ameliorates pathological hippocampal gene-expression in CamkIIδc TG mice.**

A. Schematic outline of the experimental design. B. Scheme for WGCNA analysis. C. Upper panel: Expression of RNA module 1 among the three experimental groups. \* $p < 0.05$ , Kruskal-Wallis test. Lower panel: Gene ontology analysis of genes that are part of RNA module 1. (bottom panel). D. Network representing top 30 hub genes of the gene network based on RNA module 1. E. Upper panel: RNA module 2 and its expression among the three experimental groups \* $p < 0.05$ , Kruskal-Wallis test. Lower panel: Functional annotations of the genes that are part of RNA module 2. F. Gene correlation network of the top hub genes ( $n = 30$ ) of RNA module 2. G. Left panel: Schematic outline of the analysis of microRNA-sequencing data. Right panel: Expression of microRNA module 2 amongst experimental groups. Kruskal-Wallis test. \*\* $p < 0.01$ . H. Heatmap showing significant negative correlation ( $FDR < 0.05$ ) between microRNA members of microRNA module 2 and hub genes from RNA module 2 (see Fig 5E). Error bars indicate SEM.

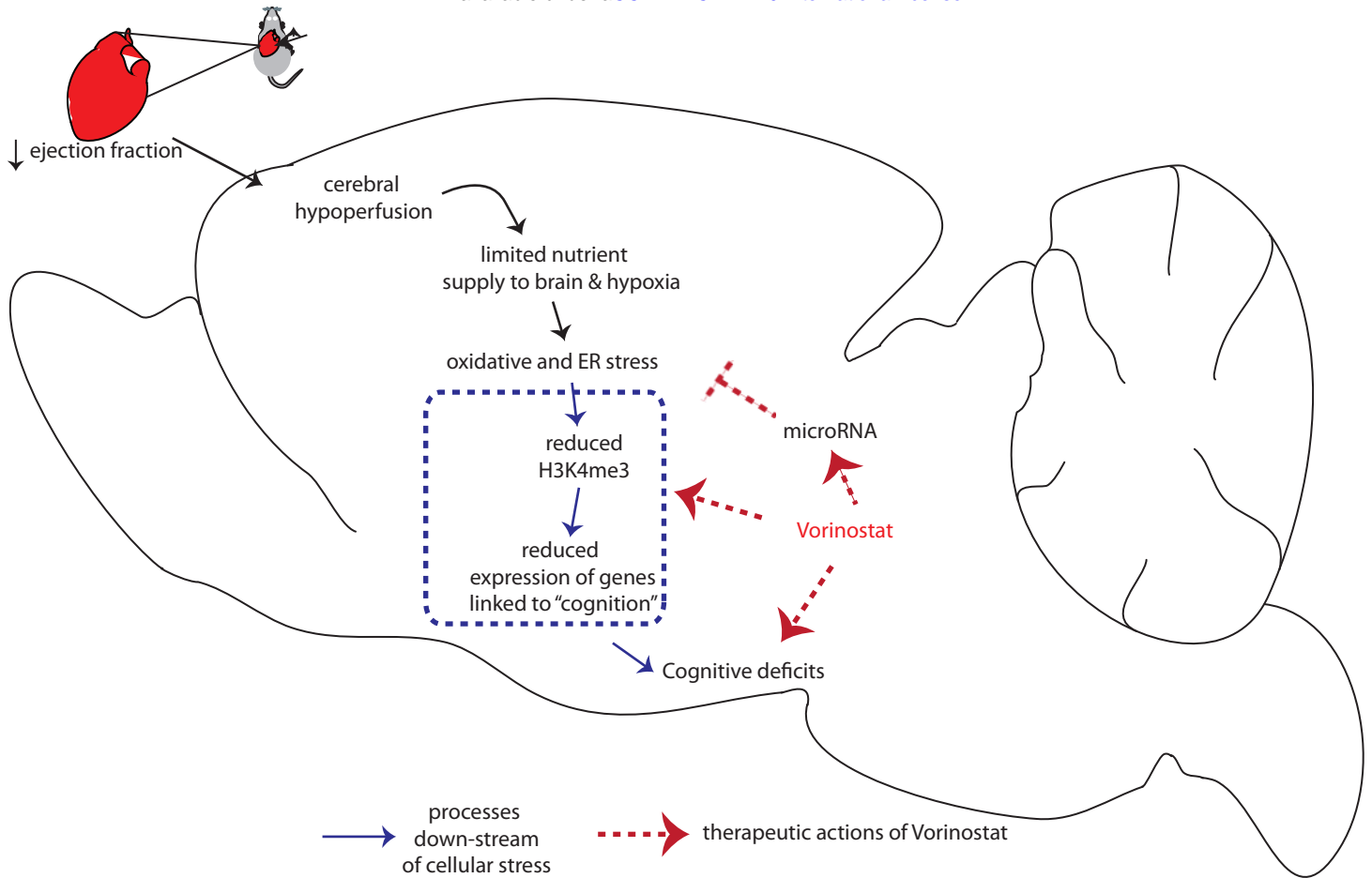
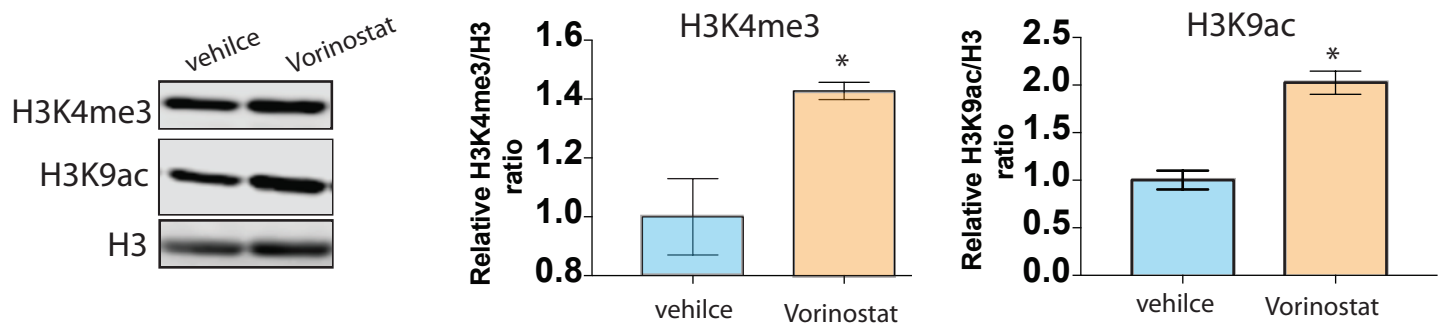


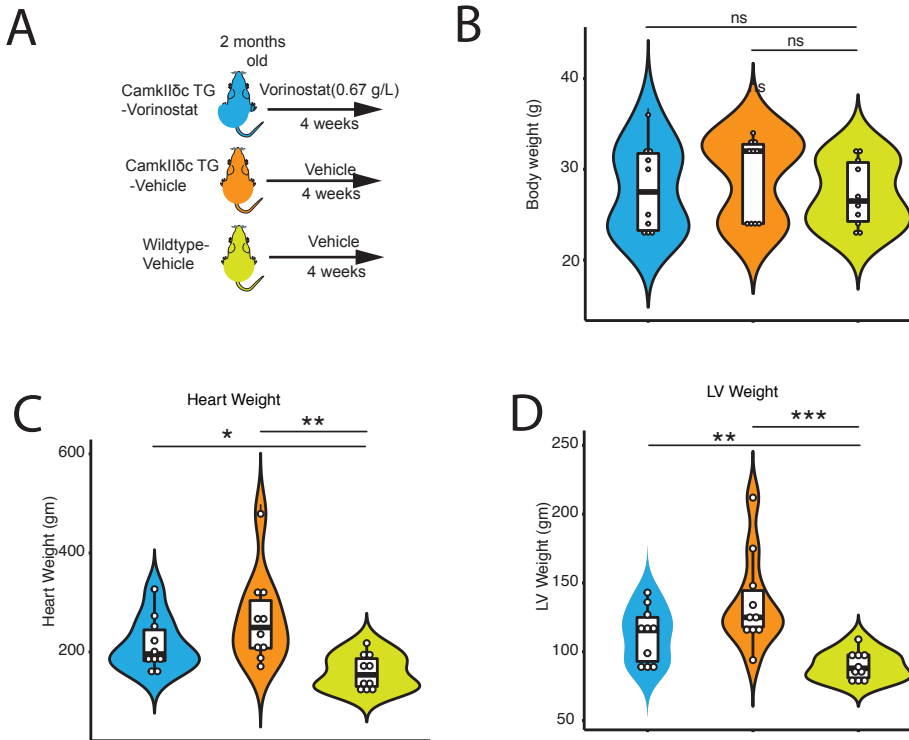
**Fig. 6. Model summarize how heart failure contributes to memory impairment and corresponding option for therapeutic intervention.** Heart failure and a reduced ejection fraction lead to cerebral hypoperfusion which is in line with a hippocampal gene-expression response linked to oxidative and ER-stress. Our data suggest that oxidative and ER-stress drive reduced expression of genes important for memory function which involves reduced neuronal H3K4me3 representation loss of euchromatin. Administration of the HDAC inhibitor Vorinostat partially increases the expression of memory-related genes but also decreases the expression of genes linked to oxidative and ER-stress via the induction of a microRNA cluster.

# Expanded view Fig 1

bioRxiv preprint doi: <https://doi.org/10.1101/2020.01.22.915637>; this version posted January 23, 2020. The copyright holder for this preprint (which was not certified by peer review) is the author/funder, who has granted bioRxiv a license to display the preprint in perpetuity. It is made available under a [CC-BY-NC-ND 4.0 International license](#).



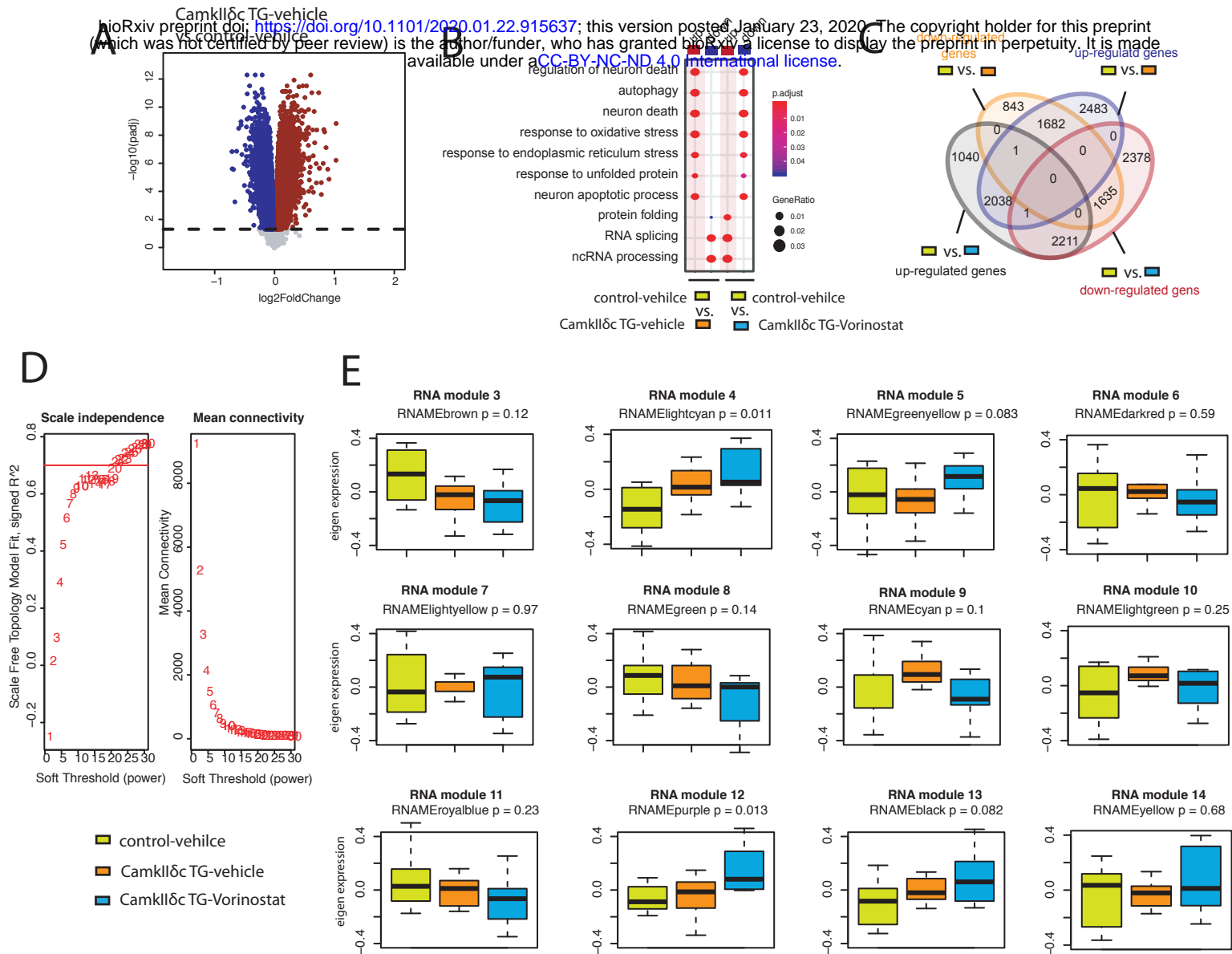
**Expanded view Fig 1: Vorinostat increases H3K4me3 level in primary neurons.** Primary mouse hippocampal neuronal cultures (10 DIV; n=3/group) were treated for 1h with Vorinostat (1 $\mu$ m) or vehicle before proteins were isolated and subjected to immunoblot analysis. Left panel: Representative immunoblot analysis. H3 was used as loading control. Right panels: Semi-quantitative analysis of immunoblot analysis from two independent experiments (n=3/group and experiment). Relative Intensity was normalized to H3 level. The data reveal that Vorinostat treatment significantly increases bulk levels of H3K4me3 and H3K9ac. \*P < 0.05, t-test; Error bars indicate SEM.



**Expanded View Fig 5: Cardiac function is not significantly affected in Camk1lδc TG mice upon Vorinostat treatment**

**A.** Scheme of the experimental design. Vorinostat treatment was initiated at 2 months of age and analysis was performed at 3 months of age.  $n = 10$ /group. **B.** Violin plot showing that body weight was similar amongst groups. **C.** Violin plots showing that heart weight and left ventricle (LV) weight (**D**) was increased in vehicle and Vorinostat-treated Camk1lδc TG mice when compared to the wild-type vehicle control group. ns; not significant,  $*P < 0.05$ ,  $**P < 0.01$ ,  $***P < 0.001$ , Kruskal wallis t-Test.

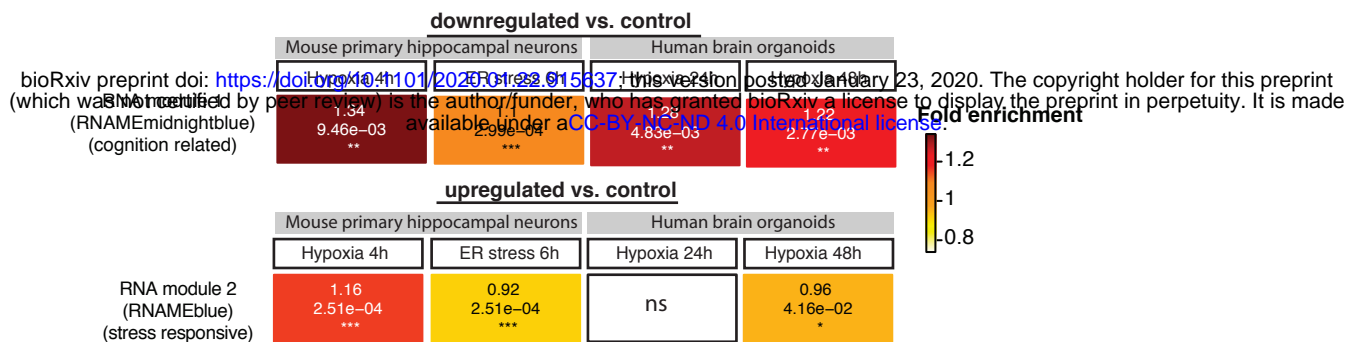
# Expanded View Fig 3



**Expanded View Fig 4: Weighted gene co-expression analysis upon Vorinostat treatment. A.** Volcano plot showing significantly deregulated genes in the hippocampal CA1 region, when comparing vehicle-treated CamkII $\delta$  Tg mice to vehicle-treated control mice (FDR < 0.05). Up- and down-regulated genes are represented in darkred and darkblue colors respectively. **B.** Pathways affected in the hippocampal CA1 region when comparing vehicle-treated wild type vs. CamkII $\delta$  mice to Vorinostat-treated CamkII $\delta$  vs. vehicle-treated wild type mice. Note that Vorinostat-treatment ameliorates pathways affected in CamkII $\delta$  TG mice for pathway increased and decreased under pathological conditions. **C.** Venn diagram showing common and uniquely deregulated genes between groups. **D.** Soft power selection based on scale independence and mean connectivity for different modules identification in WGCNA. **E.** Different modules representing distinct expression patterns among groups. Y axis representing eigen expression of given cluster/module.



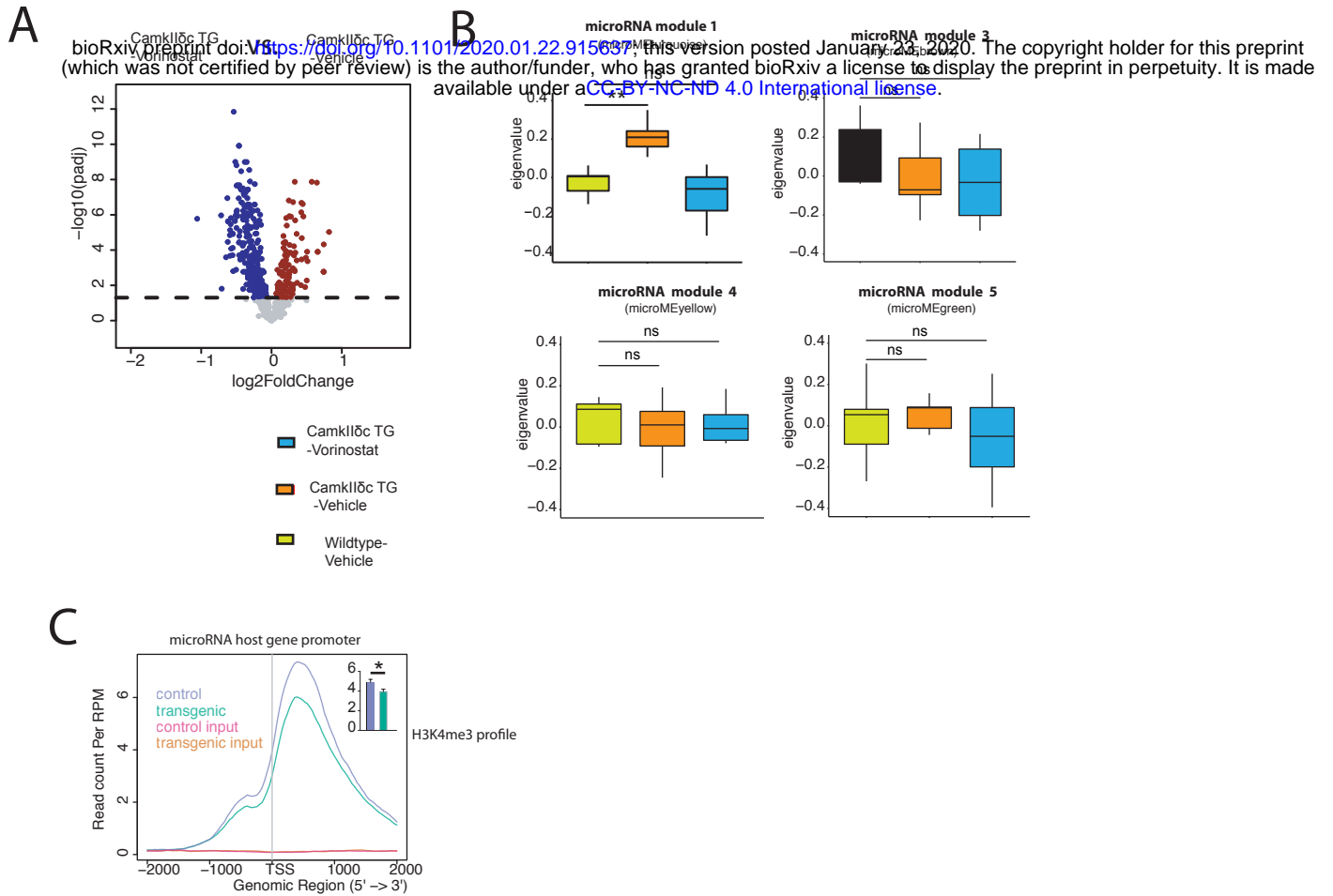
# Expanded View Fig. 4



## Expanded View Fig 4. Hypogeometric overlap analysis comparing conserved the gene-expression networks RNA module 1 and 2 to hypoxic and ER stress conditions

Heatmaps summarizing results from hypergeometric tests for genes in RNA module 1 and 2 with stress conditions in different experimental settings. Hypoxia (1% O<sub>2</sub>, 4h) and endoplasmic stress (tunicamycin 2 ug/mL, 6h) was modeled in primary hippocampal neurons. Gene expression data on hypoxia from human brain organoid data is retrieved from Pasca et al, 2019. Up and down regulated genes (FDR<0.05) were determined by comparing to corresponding controls. Enrichment significance cutoff: FDR < 0.05. Color intensity represents fold enrichment.

# Expanded View Fig 5



**Expanded View Fig 5: Vorinostat induced microRNA expression changes in the hippocampal CA1 region of CamkII $\delta$ c TG mice.** **A.** Volcano plot showing differentially expressed microRNAs when comparing Vorinostat-treated to vehicle treated CamkII $\delta$ c TG mice. **B.** Expression of microRNA modules from WGCNA analysis in three experimental groups. wild type vehicle: n = 9; CamkII $\delta$ c TG-vehicle n = 7; CamkII $\delta$ c TG-Vorinostat n = 10; kruskal wallis test. **C.** H3K4me3 profile at promoter of genes that harbor microRNAs. H3K4me3 level at promoter of these genes is significantly reduced in transgenic mice. Unpaired t-test, \*p<0.05. Error bars indicate SEM.